



**HAL**  
open science

## **In vitro three-dimensional cell cultures for bone sarcomas**

Javier Muñoz-Garcia, Camille Jubelin, Aurélie Loussouarn, Matisse Goumard,  
Laurent Griscom, Axelle Renodon-Cornière, Marie-Françoise Heymann,  
Dominique Heymann

### ► To cite this version:

Javier Muñoz-Garcia, Camille Jubelin, Aurélie Loussouarn, Matisse Goumard, Laurent Griscom, et al.. In vitro three-dimensional cell cultures for bone sarcomas. *Journal of Bone Oncology*, 2021, 30, pp.100379. 10.1016/j.jbo.2021.100379 . inserm-03298212

**HAL Id: inserm-03298212**

**<https://inserm.hal.science/inserm-03298212>**

Submitted on 23 Jul 2021

**HAL** is a multi-disciplinary open access archive for the deposit and dissemination of scientific research documents, whether they are published or not. The documents may come from teaching and research institutions in France or abroad, or from public or private research centers.

L'archive ouverte pluridisciplinaire **HAL**, est destinée au dépôt et à la diffusion de documents scientifiques de niveau recherche, publiés ou non, émanant des établissements d'enseignement et de recherche français ou étrangers, des laboratoires publics ou privés.

1 ***In vitro* three-dimensional cell cultures for bone sarcomas**

2  
3  
4  
5 Javier Munoz-Garcia<sup>1,2,#,\*</sup>, Camille Jubelin<sup>1,2,3,#</sup>, Aurélie Loussouarn<sup>1</sup>, Matisse Goumard<sup>1,2</sup>,  
6 Laurent Griscom<sup>4</sup>, Axelle Renodon-Cornière<sup>1</sup>, Marie-Françoise Heymann<sup>1,2</sup>,  
7 Dominique Heymann<sup>1,2,5,\*</sup>

8  
9 <sup>1</sup> Université de Nantes, INSERM, Nantes, France

10 <sup>2</sup> Institut de Cancérologie de l'Ouest, Saint-Herblain, France

11 <sup>3</sup> Atlantic Bone Screen, Saint-Herblain, France

12 <sup>4</sup> BIOSIT CNRS UMS3480, Université de Rennes-1, Rennes, France

13 <sup>5</sup> University of Sheffield, Department of Oncology and Metabolism, Medical School, Sheffield,  
14 UK

15  
16 # JMG and CJ contributed equally to the work

17  
18 **Running title:** 3D cultures of bone sarcomas

19  
20 **Corresponding Author:**

21 Dr Javier Munoz-Garcia

22 Email : [javier.munoz@ico.unicancer.fr](mailto:javier.munoz@ico.unicancer.fr)

23  
24 Prof. Dominique Heymann

25 Université de Nantes

26 Institut de Cancérologie de l'Ouest

27 Blvd Jacques Monod, 44805 Saint-Herblain, France

28 Email: [dominique.heyman@univ-nantes.fr](mailto:dominique.heyman@univ-nantes.fr)

29 Tel: +33 (0) 240 679 841

30

31

32	<b>Summary</b>
33	
34	1- Introduction
35	2- 3D culture methods of primary bone tumours
36	2-1 3D Osteosarcoma culture models
37	2-1.1. 3D culture and drug resistance in osteosarcoma
38	2-1.2. Impact of the tumour microenvironment structure in drug resistance
39	2-1.3. Osteosarcoma cancer stem cells and 3D culture methods
40	2-1.4. Proteomic profile in osteosarcoma 3D cultures
41	2-1.5. 3D osteosarcoma culture as a novel approach to study bone mineralisation
42	2-1.6. 3D culture methods for deciphering osteosarcoma metastatic process
43	2-1.7. Combination of 2D and 3D culture methods for the study of new vessels during
44	osteosarcoma development.
45	2-2 3D Ewing sarcoma culture models
46	2-2.1. Drug resistance in 3D Ewing cell cultures
47	2-2.2. Impact of tumour microenvironment in 3D Ewing cultures
48	2-3 3D Chondrosarcoma culture models
49	2-3.1. 3D models as tool to unravel drug resistance in chondrosarcoma
50	2-3.2. Chondrosarcoma 3D culture approaches to investigate cell adhesion, migration
51	and cell-to-cell interactions
52	3- Conclusion and future perspectives
53	
54	
55	
56	
57	
58	
59	
60	

61 **Abstract**

62 Bone sarcomas are rare tumour entities that arise from the mesenchyme most of which are highly  
63 heterogeneous at the cellular, genetic and epigenetic levels. The three main types are  
64 osteosarcoma, Ewing sarcoma, and chondrosarcoma. These oncological entities are characterized  
65 by high morbidity and mortality and an absence of significant therapeutic improvement in the last  
66 four decades. In the field of oncology, *in vitro* cultures of cancer cells have been extensively used  
67 for drug screening unfortunately with limited success. Indeed, despite the massive knowledge  
68 acquired from conventional 2D culture methods, scientific community has been challenged by the  
69 loss of efficacy of drugs when moved to clinical trials. The recent explosion of new 3D culture  
70 methods is paving the way to more relevant *in vitro* models mimicking the *in vivo* tumour  
71 environment (e.g. bone structure) with biological responses close to the *in vivo* context. The  
72 present review gives a brief overview of the latest advances of the 3D culture methods used for  
73 studying primary bone sarcomas.

74

75

76

77

78 **Key words**

79 Osteosarcoma; Ewing sarcoma; Chondrosarcoma; Extracellular matrix; 3D culture; Multicellular  
80 tumour spheroid; Scaffold-based 3D culture; Microfluidics; Bioprinting.

81

82

83

84

85

86

87

## 88 1-. **Introduction**

89 Bone sarcomas correspond to < 0.2% of diagnosed cancers registered in the EURO CARE  
90 database and then they are considered as orphan tumours. The three main types of bone sarcomas  
91 are: osteosarcoma (OS), Ewing sarcoma (ES) and Chondrosarcoma (CS). Despite their low  
92 incidence, bone tumours are associated to high morbidity and mortality, with an important impact  
93 in children and young adult population (e.g., 80% of ES patients are under 20 years of age at  
94 diagnosis). The absence of specific symptoms at early stages of the disease leads to late diagnosis  
95 that frequently corresponds to aggressive phases that include cancer cells spreading and  
96 establishment of bone and lung metastases. Unfortunately, whether the 5-year survival rate is 50-  
97 70% for OS and ES, there is a drop around 20-30% when lung metastases are detected at the time  
98 of the initial diagnostic [1]. CS are associated with high local recurrence associated with high  
99 morbidity [2].

100  
101 OS constitutes the main entity with an incidence of two-thirds of primary bone tumours and  
102 affects preferentially children and adolescents. In most of the cases, clinical treatment includes  
103 surgical procedure combined with adjuvant and neo-adjuvant polychemotherapies with or  
104 without radiotherapy. Unfortunately, distant recurrences (with a high predilection for the lung)  
105 frequently occur and are associated with drug resistance [2]. OS normally germinates from  
106 malignant mesenchymal cells of long bones committed in osteoblastic differentiation and are  
107 characterised by the production of an osteoid matrix by tumour cells [3]. The aetiology of the  
108 disease is explained by initial somatic mutations of p53, Rb and a BRACness signature that lead  
109 to chromosomal instabilities, complex genomic profile and high cellular heterogeneity [2,4].  
110 Cancer stem like cells [5], tumour microenvironment (TME) including immune infiltrated cells  
111 and extracellular matrix (ECM) that modulates tumour cell adhesion and migration are also  
112 suspected to contribute to this high heterogeneity and to the acquisition of drug resistance [6,7].  
113 Thus, due to their highly complex pathobiology and the limited access to patient samples, a better  
114 understanding of OS growth and drug development require the generation of new cell culture  
115 methods that mimic native TME of OS [8].

116  
117 ES is characterized by its high aggressiveness, fatal malignancy developed in bone and extra  
118 skeletal sites and with a rapid metastatic expansion mainly in lung. ES is the second most

119 common paediatric bone tumour affecting 3 children per million [9]. ES principally affects  
120 Caucasian patients with a slight prevalence in men than women. ES cell classically presents a  
121 round morphology, with common expression of the CD99 (MIC2) antigen and chromosomal  
122 translocation of the *EWSR1* gene to *ETS* family genes [10]. Experimental evidence suggests that  
123 ES cells may originate from undifferentiated mesenchymal stem cells (MSCs) characterized by  
124 neuroendocrine features and acquisition of *EWSR1* translocation [11,12]. In addition to  
125 conventional chemotherapies, clinical developments are focused on downstream partners of the  
126 *EWSR1/FLI1* signalling pathways [13,14]. An important feature of ES is the high resistance to  
127 chemotherapy agents, in part due to their particular MSCs origin but also to its complex TME.  
128 Reproduction of TME by 3D culture techniques results in a key progress to better understand the  
129 behaviour and drug resistance of ES.

130

131 CS compose a heterogeneous group of primary malignant tumours characterised by relative low  
132 growth ratio and the formation of hyaline cartilaginous neoplastic tissue. Depending on their  
133 malignancy, CS are classified in three grades: low-metastatic grade I, intermediate grade II, and  
134 high metastatic grade III [15]. CS are characterised by a high chemo- and radio-resistance mainly  
135 due to the presence of large amount of ECM and poor vascularity that restrict the diffusion of  
136 anticancer agents and slow down their effectiveness [16]. The importance of these features has  
137 motivated the scientific community to switch to 3D culture systems that can reproduce the native  
138 CS condition and have the potential to be a great tool for developing new therapies against CS.

139

140 Beside the genetic charge present in tumour initiation, TME has emerged as a key factor for  
141 tumour development and malignancy. For a better understanding of tumour biology, the scientific  
142 community has to reproduce, as close as possible, natural cell growth conditions [17]. During last  
143 decades, many technological progresses have been proposed to mimic native tumour biology.  
144 Whereas the first documented cell culture methods date from 1885 by Wilhelm Roux [18], the  
145 establishment of a true two-dimensional (2D) laboratory tissue culture system has been described  
146 by Ross Harrison at the beginning of the 20<sup>th</sup> century [19]. This event led to a scientific  
147 revolution in the understanding of cell behaviour during healthy and pathogenic situations. While  
148 2D cell culture techniques became standards in research laboratories for a wide window of  
149 studies and fields, they do not reproduce the dynamic evolution of tumour growth and failed to

150 mimic cell-to-cell or cell-to-microenvironment interactions. To overcome these 2D culture issues,  
151 during last decades, a variety of 3D cell culture techniques has been developed including liquid-  
152 based scaffold free methods, scaffold 3D systems and the emerging organ-on-a-chip platforms:  
153 microfluidics and bioprinting systems [20-23].

154  
155 Briefly, liquid-based scaffold-free methods are based on the prevention of cell adhesion to the  
156 cell culture container surfaces (e.g., vessels, plates) by coating them with non-adherent materials  
157 such as agar or poly-hydroxyethyl methacrylate [24]. The absence of adherent surfaces promotes  
158 cell-to-cell adhesion and formation of spontaneous spheroids. Wide variety of low/non-adherent  
159 supports are commercially available nowadays. Hanging drop technique is another liquid-based  
160 scaffold free methods that allows the production of spheroids using mono- or multi-cellular (co-  
161 cultures) approach thanks to the effect of the gravity (Figure 1) [25,26]. Low adherent supports  
162 and hanging drop methods have been also widely used to study cell organisation, embryonic  
163 development, tumour biology and tissue formation [25,27-32]. However, one of the main  
164 drawbacks of liquid-based scaffold methods is the lower reproducibility and control of the  
165 surrounding cell microenvironment.

166  
167 Scaffold 3D systems consist in a structural support that favours cell adhesion, proliferation,  
168 migration, cell-to-cell interaction and signalling [33,34]. Natural scaffolds are based on  
169 molecules that are present in the ECM such as collagen, gelatine and derivatives [35,36],  
170 complex matrix (e.g., commercial Matrigel<sup>TM</sup>) and hydrogels [37,38], and polysaccharides as  
171 alginate, chitosan or hyaluronic acid [39-43]. Whereas the main advantage of these natural  
172 scaffolds is their biocompatibility, their production and inter-batches variability are the main  
173 issues of these materials. To solve these problems, synthetic scaffolds characterised by high  
174 stability, reproducibility and biocompatibility have been developed [44]. The most used synthetic  
175 scaffolds are based on polyethylene glycol (PEG) polymer hydrogels [45-48].

176  
177 Finally, organ-on-a-chip platforms are based on microfluidic devices or 3D bio-printed systems  
178 [49-53]. Both techniques allow a precise control of the TME by applying a tuneable perfusion of  
179 media that mimics blood flow and facilitates a continuous access of nutrients, oxygen and drugs  
180 [54-56]. In addition, these systems can reproduce the complexity of tissue by adding layers or

181 compartments by co-culture of different various sets of cells in the presence of various ECM  
182 components [57-59].

183  
184 In the present review, we will focus on the different 3D culture techniques recently developed for  
185 the three main bone sarcoma entities.

## 186 187 **2- 3D culture methods of primary bone tumours**

### 188 189 **2-1. 3D Osteosarcoma culture models**

190 With a low 5-years survival rate and no improvement in the last 4 decades, OS is a rare and  
191 devastating oncological entity that affects mainly children and young adults. The complexity of  
192 the bone structure and surrounding TME imply that 2D monolayer culture stays far away from  
193 the organisation of natural tumour tissue and impairs the study OS development [60].

#### 194 195 **2-1.1. 3D culture and drug resistance in Osteosarcoma**

196 Low attachment and hanging-drop cell culture are the most frequently employed liquid-based  
197 scaffold-free method and consist in an easy 3D approach for generation of OS spheroids to study  
198 cell behaviour and drug resistance (Figure 1 and Figure 2) (Table 1). By using hanging-drop  
199 methodology, Rimann *et al.* demonstrated that spheroids produced from established cell lines,  
200 like SaOS2 or HOS, exhibited a totally different pattern of resistance to a panel of antitumor  
201 drugs compared to 2D (monolayer) culture methods [61]. Indeed, the IC50 values for  
202 doxorubicin, cisplatin, taxol, and taurolidine significantly increase in 3D culture, meaning that  
203 3D cells are more resistant to those drugs than monolayer culture. Those data were consistent  
204 with the observation done in patients where treatment based in 2D dose concentrations showed a  
205 decrease of drug effectiveness compared to 2D culture [61]. Many papers appeared reinforcing  
206 the concept that 3D spheroids are really closed to real tumour behaviour to drug treatment [62-  
207 65]. Similarly, U2OS spheroids generated by ultra-low attachment methods were used to mimic  
208 tumour structures and demonstrated the potential use of the nuclear NAD synthesis enzyme  
209 nicotinamide mononucleotide adenylyltransferase-1 (NMNAT1) as a target for anti-tumour drugs  
210 [66]. The expression of this enzyme increased in several tumour cell lines after exposure to DNA

211 damaging agents as cisplatin and doxorubicin, suggesting an important role of this enzyme in  
212 tumour resistance [66].

213

### 214 **2-1.2. Impact of the tumour microenvironment structure in drug resistance**

215 Cancer cells receive multiple signals (autocrine, juxtacrine and endocrine messages) coming from  
216 their cellular neighbours, the extracellular matrix and distant organs. By integrating all of the  
217 information, cancer cells change their behaviour, modify their metabolism and migration  
218 properties and become quiescent, or highly proliferative or resistant to drugs. TME then plays a  
219 crucial role in drug resistance [67]. Whereas hanging drop techniques have been used with  
220 success for rapidly forming tumour spheroids, this approach is far from wholly reproducing the  
221 natural TME controlling the cancer cell behaviour. 3D cell culture based on scaffold methods  
222 using natural components identified in the natural TME is one of the strategies proposed to  
223 mimic the environment of cancer cells. Interestingly, 3D scaffold are also bivalent tools not only  
224 usable in *in vitro* assays but also as support of cancer cells in *in vivo* animal experiments. The use  
225 of alginate beads is a perfect example of a 3D scaffold frequently applied to the oncology field.  
226 Alginate is used firstly to encapsulate and proliferate OS cells in a 3D spheroid configuration,  
227 and secondly for studying the metastatic effect of OS cells in animal model after inoculation of  
228 encapsulated cells [68]. The drug sensitivity was compared between 2D and 3D cell culture  
229 conditions and revealed a significant higher drug resistance when cells were cultured in 3D  
230 scaffolds compared to monolayer (2D) cell cultures. The use of silk sponges was also described  
231 as 3D scaffold for the expansion of SaOS2 and U2OS cell lines, which appeared less sensitive to  
232 drug treatment (doxorubicin and cisplatin) than cell lines cultured in a 2D environment [69]. 3D  
233 SaOS2 and U2OS cell spheroids were also generated by using commercial culture plates coated  
234 with various matrix: hyaluronic acid, collagen and adhesion proteins (Biomimesys™ matrix,  
235 from HCS Pharma, France). By using such an approach, 3D cultures differentially modulated the  
236 ATP binding cassette transporter A1 (ABCA1) and B1 (ABCB1, also known as Multidrug  
237 resistance protein-1, MDR1) expressions associated with the drug efflux and resistance which has  
238 not been observed in 2D environments [70]. 3D culture cells exposed to doxorubicin were  
239 characterized by a higher expression of ABCB1 implicated in the intracellular drug efflux,  
240 induced by the ERK1/2/HIF-1 pathway. Surprisingly, the increase of expression of ABCB1 was  
241 accompanied by a reduction of ABCA1 and by T-cell inactivation. ABCA1/ABCB1 ratio was

242 then related to the chemo- and immune sensitivity of human OS. These resistances were reversed  
243 when ABCA1/ABCB1 ratio was increased [70]. This observation suggested that the upregulation  
244 of ABCB1 transporter may induce an anti-drug and anti-immune resistance properties in OS  
245 tumours.

246 The physical characteristics (e.g. elasticity) of the scaffolds influence cancer cell properties. The  
247 generation of a hydrogel with a tuneable network of PEGDA and Gelatin-Methacryloyl (GelMA)  
248 enabled the control of the stiffness and adhesion properties of the substrate. The stiffness of the  
249 substrate correlated with the proliferation and progression of SaOS2 OS cells which proliferated  
250 much better when the rigidity of the substrate increased. This stiffness dependency relied in the  
251 regulation of the integrin-mediated focal adhesion signalling pathway [71]. Similarly, a recent  
252 study compared the viability of OS MG63 cells cultured in four different scaffolds (collagen,  
253 Matrigel<sup>TM</sup>, alginate and agarose) and demonstrated that their viability was also dependent on the  
254 scaffold elasticity [72]. Whereas cell adherence was similar for the different cell types in 2D  
255 models, ranking collagen as the best substrate followed by Matrigel<sup>TM</sup>, alginate and agarose, 3D  
256 cultures of OS cells were more dependent on substrate elasticity for an optimal proliferation. In  
257 this case, robust gels such as collagen and agarose are more proliferative substrates than softer  
258 hydrogels, Matrigel<sup>TM</sup> and alginate. Interestingly, even if the four substrates were able to produce  
259 *in vivo* tumour in animal model, tumour size and angiogenesis process also correlated to the  
260 elasticity of the substrate and showed higher size and micro-vessel formation in collagen and  
261 agarose than in Matrigel<sup>TM</sup> or alginate [72]. Mechanical properties of the ECM were also related  
262 to the drug resistance of cancer cells. Molina *et al.* developed a 3D culture system that allows  
263 mechanical modulation of TME by changing substrate stiffness [73]. They observed that lower  
264 stiffness induced the nuclear localisation of mechanotransduction pathways, contributing to  
265 specific drug resistance to anti insulin-like growth factor-1 and mTOR drugs [73]. By using  
266 collagen scaffold, Fallica *et al.* demonstrated that U2OS osteosarcoma cells exhibited increased  
267 resistance to the anti-proliferative drug PI103 in 3D gels than in conventional 2D cultures [74].  
268 These authors observed that the increase of collagen concentrations augmented the resistance of  
269 OS cells to the inhibitor. This observation was in agreement with many clinical cases in which  
270 the increase of collagen levels in TME was associated to a poor patient survival [75]. Reinforcing  
271 the importance of collagen scaffold composition, Charoen *et al.* demonstrated that concentration  
272 of 3-4 mg/ml of type I-collagen gels was crucial for optimum development of OS spheroids,

273 whereas the optimum concentration for MDA-MB-231 breast cancer spheroids was 2 mg/ml  
274 [76]. These data suggest that production of specific tumour niches depends on tissue ECM  
275 composition. Matrigel<sup>TM</sup> or agarose were replaced by methylcellulose for facilitating the  
276 development of cancer cell spheroids. Based in an *in vitro* methylcellulose scaffold model, Bai *et*  
277 *al.* generated spheroids from HOSS1 OS cell line and various soft-tissue sarcomas including  
278 HT1080 fibrosarcoma, RD rhabdosarcoma, SW872 liposarcoma cells. Spheroids formed in this  
279 3D environment showed more resistant properties to doxorubicin, gemcitabine and docetaxel or  
280 X-ray radiation than those formed in 2D cultures [77].

281  
282 Tumours are characterized by a high heterogeneity of cell distribution with a necrotic or  
283 apoptotic core surrounded by quiescent layer of cells followed by proliferative cells. This tumour  
284 stratification is associated with a different TME composition in each tumour region. The  
285 determination by mass spectrometry imaging (MSI) of the spatial distribution of metabolites in  
286 response to doxorubicin treatment on SaOS2 OS cells cultured in alginate compared to 2D  
287 underlined the role of the 3D environment. The combination of 3D culture and MSI techniques  
288 represent a new tool to better understand drug activities and design new therapeutic approaches  
289 [78]. In addition to its role in anti-tumour drug resistance, TME plays a role in cell accessibility  
290 for genetic manipulation. 3D mineralized alginate-chitosan cell encapsulation resulted in an  
291 efficient tool for gene transfection in human bone cells [79]. Polysaccharide beads facilitated  
292 gene uptake by SaOS2 cells when specific calcium phosphate and chitosan rate were used  
293 indicating that microcapsule environment composition is crucial for gene transfection in 3D bone  
294 model [79].

295

### 296 **2-1.3. Osteosarcoma cancer stem cells and 3D culture methods**

297 OS, and other tumours, are composed by highly heterogeneous cell populations that include  
298 “Cancer Stem Cells” (CSCs) or ‘tumour-initiating cells” [6,80,81]. CSCs combine stem cell  
299 features with tumour characteristics as tumour initiation ability, dormancy, recurrence and  
300 metastasis [80,82]. Thus, CSCs respond differently to anti-tumour treatments than non-CSCs  
301 tumour cells by showing a more resistant drug phenotype and leading the role of treatment failure  
302 [81]. CD133 CSC spheroids were generated from the SaOS2 cell line by using a scaffold-free 3D  
303 model based [83]. The generated spheroids were viable, conserved their pluripotency, and

304 constituted an ideal model for drug screening. CSCs enrichment from MG-63 and SaOS2  
305 spheroids by scaffold-free method was combined with two hybrid scaffolds that mimic ECM and  
306 used to analyse the impact of ECM in OS CSCs development [84]. Hybrid scaffold was  
307 constituted by Mg-doped hydroxyapatite coupled to collagen fibres and a porous hydroxyapatite  
308 substrate. Both hybrids scaffolds resulted in stable CSCs enriched OS spheroid growth without  
309 any loss of round morphology compared to 2D. Moreover, an increase of stemness markers  
310 including OCT-4, NANOG and SOX-2 was observed that indicated that both types of hybrids  
311 scaffolds were able to mimic native environment promoting CSC stimulation [84].  
312 Hydroxyapatite nanoparticle 3D cultures had a strong impact on the survival of OS cells under  
313 anti-tumoral oxidative stress therapy [85]. Cold atmospheric plasma resulted in a potential  
314 therapy in OS by induction of oxidative stress and subsequently cell death in 2D cultures.  
315 However, when this therapy was tested in 3D, MG-63 OS cell cultures in hydroxyapatite  
316 nanoparticles were characterised by a significant decrease of cell death [85]. This property was  
317 related to 3D environment due to the nanoparticles that favoured cell scavenging and evasion  
318 from reactive oxygen and nitrogen particles. Moreover, the generated 3D TME enhanced CSCs  
319 subpopulation expansion [85]. These data suggest a relevant role of TME in the development and  
320 drug resistance of CSC on OS, and the advantage of the use of 3D culture techniques that mimic  
321 native 3D OS nature unlike 2D approaches.

322

#### 323 **2-1.4. Proteomic profile in osteosarcoma 3D cultures**

324 Protein expression and modification are highly impacted by nutrient availability and TME.  
325 Interestingly, the protein expression profiles significantly differ between 2D and 3D culture. A  
326 proteomic study using spheroids produced by ultra-low attachment supports from the dog OS cell  
327 line D17 demonstrated that the development in 3D culture induces an increase of  
328 glycolysis/gluconeogenesis pathways, biosynthesis of amino acids and changes in carbohydrate  
329 metabolism [86]. These data were in agreement with the metabolism observed during tumour  
330 development and the generation of a hypoxic local environment. Chaperon's family, which is  
331 composed by protein folders associated to cellular stress response and cytoskeletal organization,  
332 is similarly modulated by 3D context. On the opposite manner, general protein phosphorylation is  
333 upregulated in 2D cultures compared to 3D environment, probably due to the increase in the  
334 growth rate observed in monolayer cell cultures [86]. These data suggest that, in order to better

335 understand the proteomic profiles presented in tumours, all the previous information obtained by  
336 2D studies must be re-evaluated in the light of the 3D culture methods close to the tumour  
337 behaviour.

338

339

#### 340 **2-1.5. 3D osteosarcoma culture as a novel approach to study bone mineralisation**

341 OS is characterised by the production of mineralised tissue. Osteoblastic-like OS cells show an  
342 increase in the level of protein implicated in the mineralisation process (as TNAP, BMP-2 and  
343 CaSR). The faster osteogenic properties of OS cells make them an interesting tool to better  
344 understand the bone mineralisation process. While 3D culture techniques have been widely  
345 developed for mimicking TME and, subsequently, more reliable anti-cancer drugs screening,  
346 bone 3D cultures were also used to study osteogenesis biology.

347

348 Natural and synthetic scaffold gels generate a macro- and microstructural configuration similar to  
349 the trabecular bone identifying these materials as perfect supports to study bone mineralisation  
350 [87-89]. Type I collagen stands out as a great 3D scaffold for bone mineralisation in which  
351 SaOS2 cells can be expanded. Magnesium is a key cation involved in many biological activities  
352 such as metabolism, muscle contraction and bone cell function. Almost 50% of the magnesium  
353 present in the body is associated with bone tissue (hydroxyapatite crystals, HA) and influences  
354 bone-remodelling processes. By using a 3D collagen scaffold approach, Picone *et al.* showed that  
355 intracellular magnesium was incorporated at the early phase of bio-mineralisation, a process  
356 which may favour HA platelet formation and interfibrillar mineralisation [90]. The composition  
357 of culture media appeared critical similarly to the 3D environment. Indeed, a Modified Eagle's  
358 Medium resulted in a better mineralisation induced by SaOS2 than conventional medias (e.g.  
359 Dulbecco's Modified Eagle's Medium) used for this cell line [91].

360

361 The morphology of mineralised matrix produced by HOS OS cells strongly differed according  
362 the cell culture condition used (2D to 3D) [92]. While 2D cell cultures produced spheroid  
363 particles in the surrounding cell layers, in 3D culture conditions (type I collagen and poly-ion  
364 complex hydrogels) amorphous mineralised particles were observed at the matrix layers. This  
365 phenomenon produced gel turbidity that could be used as an indicator of the level of

366 mineralisation [93-95]. These data indicate that 3D gels are interesting approaches for  
367 osteogenesis studies associated with OS development. However, structure and mechanical  
368 properties of 3D gels are crucial parameters for investigating bone mineralisation. Similarly to  
369 tumour development, the pore size of the matrix used to promote osteogenesis is a critical factor.  
370 Using bioprinting approach, Vanderburgh *et al.* showed that a 300  $\mu\text{m}$  pore size produced the  
371 optimum osteoblast differentiation and mineralisation. In addition, this pore size also favoured  
372 OS tumour growth and proliferation [96]. The distribution of pores also influences the structure  
373 of the extracellular matrix. The comparison of two types of 3D poly(D,L-lactic acid) scaffolds,  
374 one with regular pore distribution and the other with random distribution, showed that both types  
375 were adapted substrates for the attachment and proliferation of MG63 OS-derived osteoblasts.  
376 However, the random pattern, which is closer to real bone structure, induced a better distribution  
377 and organization of collagen fibres [97]. Polydimethylsiloxane (PDMS) is widely used as  
378 material to produce microfluidic devices but it can be also used as a scaffold for cell cultures  
379 [98]. A water-PDMS emulsion was used as a porous template for SaOS2 OS proliferation.  
380 Playing with different curing parameters for PDMS and pressure, Riesco *et al.* generated various  
381 grades of PDMS reticulation that allowed proper adhesion and proliferation of OS cells.  
382 Moreover, this system provides a fast and cheap way to produce scaffolds in mass [98]. As  
383 mentioned before, PDMS is the most commonly used material for microfluidic device fabrication  
384 (Figure 3). A microfluidic chip was developed for the production of OS spheroids in mass (up to  
385 5000) [99]. Microfluidic device was treated with a surfactant (Synperonic®) to generate a non-  
386 adherent surface that favoured the generation of MG63 spheroids in a similar way as non-  
387 adherent plates. Massive production of spheroids was used to challenge spheroids to two different  
388 cellular stresses: nutrient deprivation (serum concentration) and hypoxia (HIF inhibition). 3D  
389 cultures obtained data confirmed *in vivo* observation where stress conditions favoured the  
390 increase of VEGF secretion and induction of malignancy processes [99]. This study confirmed  
391 the impact of ECM variation in tumour malignancy as well as demonstrated that microfluidic  
392 approaches represent an interesting tool for massive 3D cultures and analysis. However, it has  
393 been reported that the combination of commercial OS tumour cell lines and collagen and  
394 Matrigel<sup>TM</sup> scaffolds may not be the perfect model for 3D tissue bone engineering studies [100].  
395 The hypoxia observed in 3D cultures using scaffolds like collagen and Matrigel<sup>TM</sup> generated less  
396 oxidative stress by tumour cells than in 2D. In addition, this oxidation can negatively impact the

397 bone mineralisation [100]. By using non-tumour cell lines, Gamblin *et al.* generated 3D cultures  
398 to study osteoblastic and osteoclastic differentiation [101]. Based on biphasic calcium phosphate  
399 microbeads scaffolds, these authors induced the proliferation of MSCs that adhered and  
400 proliferated with abundant production of collagenous ECM. Interestingly, the system promoted  
401 the co-cultures of differentiated MSCs with osteoclasts generated from peripheral blood CD14-  
402 positive monocytes. Altogether, the system was able to mimic bone precursors behaviour and  
403 established a valid non-tumour approach to study drugs for bone healing, osteoporosis and OS  
404 biology [101]. The production of hybrid scaffolds as the combination of layers of biodegradable  
405 polymer poly( $\epsilon$ -caprolactone) (PCL) and layers of chitosan in combination with HA by  
406 electrospinning method resulted in continuous micro- and nano-fibers with high surface area and  
407 micropores that provided optimal attachment and proliferation of SaOS2 OS cells with high  
408 mineralisation activity [102]. Bioprinting methods have been also used to produce hybrid  
409 hydroxyapatite-chitosan-genipin hydrogels to analyse nanomechanical properties of generated  
410 bone tissue [103]. Bioprinter hybrid scaffolds resulted in a good structured TME that favoured  
411 3D MG63 OS cell adhesion, culture and proliferation [103], indicating that bioprinting methods  
412 constitute interesting platforms to analyse how the composition and architecture of ECM impact  
413 bone mineralisation.

414  
415 Other types of scaffold methods for 3D culture of OS cells imply the use of stirred-tank  
416 bioreactors [104]. Base on this equipment, Chen *et al.* developed a fibrous bed bioreactor with a  
417 3D polyester fibrous matrix that resulted in a better production of 143B OS spheroids compared  
418 to 2D cell cultures. Moreover, they gave evidence that a 3D scaffold favoured the retention of  
419 viable and non-apoptotic tumour cells together with a long-term stability [104].

420

### 421 **2-1.6. 3D culture methods for deciphering osteosarcoma metastatic process**

422 OS cells are characterized by their ability to spread to distant tissues forming metastases (lung  
423 and bone) as carcinomas. To understand the process of cell dissemination and metastasis  
424 development, 3D bone tissue cultures were produced using a microfluidics device to mimic and  
425 analyse the “metastatic” installation in bone [105]. Hao *et al.* [106] developed a bone-on-a-chip  
426 microfluidic device in which they generated mature osteoblastic tissue using the  
427 MC3T3osteoblast precursors cell line. Cells produced a layer of heavily mineralised collagen

428 fibres up to 85  $\mu\text{m}$  in thickness. By using this system, they analysed similarly the capability of  
429 metastatic breast cancer cell line (MDA-MB-231) to invade bone tissue. After 14 days of co-  
430 culture, cancer cells seeded and invaded the apical layer of mineralised bone tissue in an “Indian  
431 file” and formed “micro-metastases” [106]. Choudhary *et al* developed an interesting  
432 microfluidic PDMS device that contained culture chambers in which primary human osteocytes  
433 were cultured in the presence of collagen-coated biphasic calcium phosphate microbeads for  
434 producing bone tissue in hypoxic conditions. Co-culture of conditional reprogrammed prostate  
435 cancer cell line (PCa3) with 3D osteocyte culture induced an increase of fibroblast growth factor-  
436 23, RANKL mRNA expression levels and alkaline phosphate activity by osteocytes that was  
437 associated to an increase of the mineralisation process. These results suggested that 3D  
438 microfluidic devices can be useful to better understand the metastatic process induced by primary  
439 tumours in bone tissue [107]. 3D microfluidic devices were also used to analyse the cell traction  
440 force in confined TME [108]. This device consisted in deflectable PDMS microspots included in  
441 micro-channels with different wide cross-sections. Migration test using HOS OS cells  
442 demonstrated that, in contrast to what observed in non-confining microchannels, tumour cell  
443 traction forces did not depend on myosin-II. This result showed that migration mechanisms of  
444 tumour cells during metastasis can vary depending on tissue structure, which compromises anti-  
445 metastatic drug approaches. Moreover, the traction force devices resulted in an appealing  
446 approach for new anti-metastatic drug selection screening [108].

#### 447 448 **2-1.7. Combination of 2D and 3D culture methods for the study of new vessels during** 449 **osteosarcoma development**

450 An alternative to the development of complex 3D micro systems is the combination of 2D and  
451 3D cultures. To study angiogenesis process during tumour development, 3D MG-63 OS  
452 spheroids were generated by hanging drops using Gravity PLUS plates, reaching a size of 400  
453  $\mu\text{m}$  in diameter, and co-cultured with a HUVEC endothelial monolayer [109]. MG-63 OS  
454 spheroids produced similar ECM compared to *in vivo* tumours and acquired similar tumour  
455 architecture with proliferation cells at the periphery and quiescent cells at the centre of the  
456 spheroids. The generation of a hypoxia compartment induced the production of VEGF factor by  
457 tumour cells promoting proliferation and differentiation of HUVEC to produce vascular tubule-  
458 like structures. Using dog OS cell lines (D22 and D17) and 3D collagen gels, Massimini *et al.*

459 demonstrated that a non-human OS model was associated with induced vasculogenic mimicry  
460 and that 17-AAg drug abolished tumour progression and micro vascular channel formation [110].

461  
462 **2-2. 3D Ewing sarcoma culture models**

463 ES is the second most common paediatric bone malignancy and the third most frequent primary  
464 bone sarcoma after OS and CS. In addition to the *EWS/ETS* fusion gene which is at the origin of  
465 the disease, numerous investigations highlighted the contribution of the TME in the progression  
466 and malignancy of ES [111]. Similarly to OS, scientific community has put their effort to set up  
467 new *in vitro* ES models (Table 1).

468  
469 **2-2.1 Drug resistance in 3D Ewing cell cultures**

470 Electrospun polymeric scaffolds based on the inert polymer PCL have become a promising 3D  
471 platform to study mechanistic and drug resistance processes in TC-71 ES cell line. TC-71 3D  
472 culture reproduced morphology, proliferation and protein expression similar to observations in  
473 human tumours. As remarked in OS models, a 3D configuration induces more resistance to drug  
474 treatment (doxorubicin) than 2D cultures [111,112]. Interestingly, the PCL 3D model revealed  
475 that the IGF-1R/mTOR signalling pathways were highly activated in ES 3D models and these  
476 pathways played a key role in the upmodulation of tumour cell adhesion, identifying IGF-  
477 1R/mTOR signalling pathways as new potential targets for drug treatment in ES [111]. Similarly,  
478 Santoro *et al.* emphasized the role of IGF1/IGF-1R pathway and biomechanical TME stimulation  
479 in drug resistance by using similar 3D models [113]. These data are in agreement with the recent  
480 study published by Molina *et al.* [114]. Indeed, these authors demonstrated that 3D TME  
481 favoured the downregulation of IGF-1R via mTOR pathway, which was accompanied by a  
482 reduction of the clathrin-dependent nuclear localisation and transcription activity of IGF-1R  
483 [114]. TC-71 3D culture was exposed to different shear stresses close to those observed in bone  
484 microenvironment in a flow perfusion bioreactor. Under shear stress, 3D ES cells enhanced cell  
485 tumour proliferation and induced an increase of IGF1 pathway compared to 2D cultures. Besides,  
486 the increase of IGF1 levels was associated to the resistance to dalotuzumab (an inhibitor of IGF1  
487 receptor) and the downregulation of the c-KIT and HER2 oncoproteins [113]. These data  
488 suggested that biomechanical forces impacted the progression and malignancy of ES cells [113].  
489 When ES spheroids were grown in a 3D mimic bone tissue, there was an increase in ERK1/2

490 phosphorylation and RUNX2 protein levels associated to drug resistance that was not observed  
491 when the same cells were cultured in 2D [115]. Interestingly, an increase of RUNX2 level was  
492 similarly observed in patients suffering from ES [115]. All those data suggest that ECM displays  
493 a key role in ES drug resistance by induction of specific mechanotransduction signalling  
494 pathways including RUNX2.

495

### 496 **2-2.2. Impact of tumour microenvironment in 3D Ewing cultures**

497 ES are characterised by a rapid development of multidrug resistance due to the overexpression of  
498 Multidrug resistance associated protein-1 (MRP1) and ABCB1 [116]. Similarly to OS, the drug  
499 resistance of ES cells was also related to a set of stem cells with tumour-initiating properties with  
500 a development dependent of TME [116]. Supporting this idea, ES spheroids produced by ultra-  
501 low attachment method under serum-free conditions failed to generate tumour-initiating cells  
502 [117]. Although ES cells (VH-64, TC-32, TC-71 and A4573) form spheroids in serum-free  
503 media with a diameter ratio of 200 µm and with phenotypes similar to 2D cultures, none of them  
504 was able to self-renew or expand in a clonogenic manner indicating that TME is a key factor for  
505 ES enrichment [117]. Reinforcing the role of TME in ES development, Villasante *et al.*  
506 developed an interesting 3D model based on the combination of an engineered bone tissue with  
507 spheroids produced from different ES cell types (RD-ES, SK-N-MC and EWS-GFP) [118]. Bone  
508 tissue was generated from induced osteogenic differentiation of human MSCs in a native bone  
509 ECM, whereas ES spheroids were formed thank to the intrinsic nature of ES cells to generate cell  
510 aggregates after long period of culture (one week at 37°C in Eagle's Minimum Essential Medium  
511 supplemented with 10% Hyclone FBV [119]). The co-culture of these ES spheroids in the tissue  
512 bone matrix recapitulated the tumour behaviour, including the re-expression of focal adhesion  
513 and related cancer genes, generation of a hypoxic and glycolytic phenotypes and development of  
514 angiogenesis potential [118]. This study pointed out the requirement of specific niche  
515 configuration for proper development of ES. Reproduction of hypoxic conditions is indeed  
516 necessary to better understand how tumours develop angiogenic mechanism. Agar coated plates  
517 were used to induce A673 ES spheroids that were moved to a hypoxia chamber for analysing the  
518 functional relationship between hypoxia, spheroid cell distribution and DNA damage response  
519 [120]. Under hypoxic conditions, A673 ES spheroids displayed a stratification of cellular  
520 population from necrotic cells at the nucleus of the spheroids to proliferating cells located at their

521 surface. Moreover, cells localized at the nuclear and perinuclear zone of the spheroids were  
522 characterised by an increase of  $\gamma$ -H2AX via the ATM DNA repair pathway, indicating that this  
523 approach can be used for anti-ATM drug development in ES [120]. Recently, a new approach  
524 was described for encapsulation in alginate spheres of ES cells isolated from patient derived  
525 xenografts without losing their phenotype [121]. While ES primary cultures were maintained for  
526 at least one month, cells at the core of spheroids did not undergo to hypoxia which is a key step  
527 of tumour angiogenesis. That could be due to the limitations in spheroid size by the alginate  
528 beads tested (<200  $\mu$ m), as hypoxia has been observed when spheroids reach a size over 400  $\mu$ m  
529 [122]. Overall, this method has an interesting potential as drug screening platform and can be  
530 easily implemented for hypoxia studies. In addition, encapsulation of different cell types in  
531 alginate beads can be a useful tool for cell-to-cell interactions in ES.

532

### 533 **2-3. 3D chondrosarcoma culture models**

534 CS is the second most frequent bone cancer characterised by the production of malignant  
535 cartilaginous matrix [123,124]. Surgery is the only effective medical treatment as CS are  
536 characterised by a high resistance to chemo- and radiotherapy. However, the mechanisms that  
537 control and regulate CS differentiation are still not well defined. MSCs can undergo into  
538 chondrogenic differentiation and have been used to understand the gene expression that  
539 determine 3D chondrogenic mechanism [125]. Chondrogenic differentiation of MSCs was  
540 associated to an increase of *SERPINA1* and *SERPINA3* mRNA expression. Moreover, secretion  
541 of SERPINA-1 correlated with chondrogenesis and dedifferentiation during chondrocyte  
542 expansion, suggesting that SERPINA1 could be considered as a marker of chondrocyte  
543 differentiation [125]. Similarly, MSCs were used for studying chondrocyte differentiation in  
544 spheroids and simultaneous gene expression profiles to determine genes implied in pre-  
545 chondrogenic and chondrogenic phenotype compared to tumour samples [126]. Comparative  
546 gene analyses allowed the identification of two clusters that mainly include ECM components,  
547 remodelling matrix enzymes and few growth factors useful to predict the clinical behaviour of CS  
548 subtypes [126].

549

550

551

### 552 **2-3.1. 3D models as tool to unravel drug resistance in chondrosarcoma**

553 As mentioned above, CS are resistant to conventional chemotherapies. CS cell resistance can be  
554 explained in part by the structure of the tissue and its dense hyalin ECM composition, indicating  
555 that 3D models will become crucial tools to better understand the mechanism underlying CS drug  
556 resistance (Table 1). Comparison study between 2D and 3D chondrogenic spheroids from  
557 different origins (SW1353, CAL78 and OUMS27) and new established CS cell line from primary  
558 tumour biopsy (CH03, CH34 and CH56) showed that 3D CS spheroids were more resistant to  
559 chemotherapeutic drugs (Doxorubicin and Mafosfamide) than 2D cultures [127]. As shown by  
560 RT-qPCR, these cell lines cultured in 2D cells lost expression of several genes (*COL2A1*, *COMP*,  
561 *ACAN*) implicated in cartilage development that was restored in 3D cultures. Moreover, the  
562 capacity of each cell type to produce cartilaginous matrix was directly related to its drug  
563 resistance [127]. These data suggested a direct functional relationship between cartilaginous  
564 matrix composition and chemoresistance. Similarly, spheroids produced by CH2879, OUMS27  
565 and L835 cell lines were used to determine the mechanism involved in resistance to cisplatin and  
566 doxorubicin [128]. 3D spheroids were generated by differentiation of cell lines after long period  
567 of culture (6 weeks in chondrogenic medium, see [129]) and exhibited CS phenotype. Exposure  
568 to chemotherapy agents highly activated the multi-drug resistance pump (ABCB1) in all CS 3D  
569 spheroids. Inhibition of the anti-apoptotic BCL-2 family members by specific drug (ABT-737)  
570 resulted in a sensitization of 3D CS to doxorubicin. These results indicated that tumour drug  
571 resistance does not rely only on ECM composition and that other mechanisms must be implied  
572 and be considered as potential targets for development of new CS therapies. Taken together,  
573 these data demonstrated that the mimicking of the cell behaviour and ECM of CS is the added  
574 value of 3D cultures. As discussed for OS, non-adherent surface methods can be used for  
575 obtaining multicellular tumour spheroids. Combination of non-adherent plates and 0.5%  
576 methylcellulose generated CS spheroids from the HEMC-SS cell line [130]. HEMC-SS spheroids  
577 developed CS tumour features as proliferative cell population at the periphery of a hypoxic and  
578 apoptotic core, with ECM rich in glycosaminoglycans and VEGF excretion (figure 4). Moreover,  
579 this model recapitulated the drug resistance phenotype observed in CS tumour for classical  
580 chemotherapy agents [130]. While still far for native tumour environment, the absence of  
581 complexity to generate this 3D system and its close features to the *in vivo* tumours make it a  
582 convincing model for massive drug screening. In this way, HEMC-SS spheroid model was used

583 to evaluate the effect of new hypoxia-activated pro-drugs that target the rich proteoglycan ECM  
584 of CS [131]. This study showed that quaternary ammonium, which is characterised by a positive  
585 charge that interacts strongly with the negative charges present in the proteoglycans [132], could  
586 be used as an adjuvant for CS drug targeting [131]. Generation of CS 3D cultures by similar  
587 hanging-drop methods showed the potential of the ionophore salinomycin (SAL) as a new anti-  
588 CS drug [133]. SAL resulted in a strong cytotoxic effect in both 2D and 3D SW1353 (grade II)  
589 CS model by inducing cellular apoptosis via caspase activation [133]. Another approach to  
590 produce 3D CS system consists in the use of natural or synthetic material that can serve as  
591 substrates for the formation of tumour mass cells in cartilage or chondrosarcoma niches. Alginate  
592 hydrogels were used to analyse the invasion and drug resistance of CS models [134]. Compared  
593 to other biomaterials as collagen and Matrigel<sup>TM</sup>, alginate is characterised by an inert and stable  
594 composition, which is translated in a more reproducible method to generate beads for  
595 encapsulation. Alginate encapsulated CH2879, JJ012 and SW1353 CS cell lines, compared to a  
596 2D culture, were characterised by a long-term lifespan with generation of a hyaline-like cell  
597 matrix and demonstrated that 3D cultures recapitulated cell matrix gene expression. Interestingly,  
598 CH2879 cell line displayed an evasion phenotype from the beads compared to the other cell line  
599 models. This was somehow in coherence with the grade of malignancy III of this cell line  
600 whereas the other two are grade II. This data suggests that alginate beads are useful to analyse CS  
601 cell invasion properties. Thus, it can be combined with drug screening as alginate beads CS 3D  
602 model summed up the characteristic drug resistance phenotype of CS cell lines [134]. In  
603 agreement with this result and by using same methodology, Palubeckaite *et al.* showed that CS  
604 3D spheroids reproduced similar phenotype that *in vivo* CS with production of an ECM enriched  
605 in collagen II and resistance to chemotherapeutic agents as doxorubicin, cisplatin, temozolomide  
606 and YM-155 [135].

607  
608 CS are resistant to radiotherapy. Hamdi *et al.* developed a 3D approach to analyse the impact of  
609 linear energy transfer ionizing radiation (LET) in CS [136]. Due to its relative photon radio-  
610 resistance, metastatic potential and cartilage phenotype, intermediate-grade II SW1353 CS cell  
611 line was used as a model. 3D culture was performed by using a collagen scaffold and hypoxic  
612 conditions (2% of O<sub>2</sub>) to mimic *in vivo* cartilage environment. Exposition to low and high LET  
613 radiation showed that 3D cultures resulted in a more resistant phenotype with a delayed response

614 of DNA repair mechanisms (evaluated by H2AX expression post radiation) than 2D cultures,  
615 where cell were grown in monolayer conditions and normoxia (20% oxygen). The main  
616 difference between culture methods relied in the microenvironment conditions, which implied  
617 that the microenvironment played a key role in the radiation resistance of CS and should be  
618 considered when determining the depth-dose profile in radiation therapy of SC [136].

619  
620 **2-3.2. Chondrosarcoma 3D culture approaches to investigate cell adhesion, migration and**  
621 **cell-to-cell interactions**

622 3D CS cultures were used to determine the impact of TME charges during cell adhesion [137].  
623 Titanium beads from 400-500 µm were modified by deposition of polyelectrolyte multilayer film  
624 that conferred a positive or negative surface charge. In the presence of negative charges, human  
625 HCS-2/8 CS cells exhibited cytoplasmatic stress fibres that were totally absent when positive  
626 charged TME were tested, indicating that anionic charges affected cytoskeleton organisation.  
627 Moreover, anionic but not cationic surfaces promoted two modes of pseudopod formation by  
628 HCS-2/8 cells, in a random progression and as a “cell recognition signal”. This phenomenon was  
629 associated with a cellular mechanism to optimize the anchoring process. Interestingly, cells  
630 developed pseudopods on cationic surfaces when cells were cultured in the presence of  
631 conditioned medium obtained from an anionic culture, suggesting that this process was regulated  
632 by an exocytotic mechanism. This mechanism was linked to the MAPK ERK1/2 pathways as  
633 phosphorylation levels were increased in the presence of anionic charges and reduced when  
634 cationic surfaces were assessed [137]. Overall, these studies suggested that ECM has a relevant  
635 role in CS cell adhesion and migration.

636  
637 As described for OS, direct or indirect cell-cell interactions between CS cells and cells of the  
638 local microenvironment can be analysed by combination of 3D and 2D cultures. In a recent study,  
639 Minopoli *et al.* analysed the contribution of pro-tumoral M2 macrophages to CS development  
640 [138]. Primary CS cells were isolated from patient biopsies and cultured by hanging drop  
641 methods to produce 3D spheroids and then co-cultured in collagen/fibroblast matrix with blood  
642 isolated monocytes. The size of CS spheroids increased in the presence of monocytes, probably  
643 due to an increase of CS cell invasive capability induced by monocyte factors. And reciprocally,  
644 CS cells induced monocyte differentiation into a pro-tumoral M2 phenotype. These observations

645 indicated a crosstalk between CS cells and macrophages through soluble mediators [138]. The  
646 induction of CS proliferation by macrophages was inhibited by the addition of urokinase receptor  
647 (uPAR)-derived synthetic peptide RI-3 which was known to reduce the monocyte migration  
648 [139]. In this context, RI-3 could potentially avoid the recruitment of monocytes to CS niches  
649 and reduce proliferation and angiogenic properties of CS tumour [138].

650  
651 Recently, an innovative method was developed to assemble 3D CS spheroids by levitational  
652 forces by using low doses of gadobutrol salt [140]. As biological tissues are considered to be  
653 diamagnetic, they can be levitated when paramagnetic medium is used. Paramagnetic ions of  
654 Gadolinium(III) ( $Gd^{3+}$ ) have been widely used as a contrast agent but are characterised by  
655 cytotoxicity at high concentrations and lower concentration of  $Gd^{3+}$  did not allow cell levitation.  
656 However, by using high magnetic fields, Parfeno *et al* induced SW1353 CS spheroid magnetic  
657 levitational bio assembly in the presence of lower doses of gadobutrol (0.8 mM). The study  
658 revealed minimal cytotoxicity by the magnetic field and opens a new area in the domain of  
659 microgravity and tumour biology [140]. In the meantime, further studies may be needed to  
660 determine if high magnetic fields have an impact in cell behaviour, genomic and proteomic  
661 expression pattern.

662  
663 **3-. Conclusion and future perspectives**

664 Primary bone tumour progression and metastasis rely on the particular combination of bone MSC  
665 differentiation and physiological, structural, biochemical TME interactions. 2D cultures were  
666 considered for a long time as a valid approach for improving the knowledge in tumour biology.  
667 Many studies gave evidence that 2D cultures did not reflect the real nature of tumours, as many  
668 treatments that were effective in 2D failed in clinical trials. In this context, development of 3D  
669 culture approaches that mimic TME is a new perspective. In particular, the use of natural  
670 materials already presents in the bone ECM or synthetic materials as scaffolds for 3D bone  
671 culture generation demonstrates to be promising approaches for the study of tumour invasion,  
672 metastasis, angiogenesis processes and anti-tumour drug development. Moreover, the  
673 development of novel technologies in 3D cultures as microfluidics and bioprinting that allow the  
674 generation of customizable 3D systems constitute a fully scientific revolution. These technologies  
675 can be combined with other 3D techniques and allow the creation of a fully controlled TME that

676 reproduces the native configuration of bone tumours, including cell-to-cell or tissue interactions,  
677 cell adhesion, proliferation and migration, EMC structure and composition, physiology  
678 parameters as hypoxia, shear stress and mechanical forces. This 3D technological revolution will  
679 be an excellent opportunity for the identification of new bone therapeutic targets and drug  
680 discovery in bone sarcoma field.

681

## 682 **References:**

683

684 [1] Ferguson JL, Turner SP. Bone Cancer: Diagnosis and Treatment Principles. *Am Fam*  
685 *Physician*. 98 (2018) 205-213. PMID: 30215968.

686

687 [2] Brown HK, Schiavone K, Gouin F, Heymann MF, Heymann D. Biology of Bone Sarcomas  
688 and New Therapeutic Developments. *Calcif Tissue Int*. 102 (2018) 174-195. [https://doi:](https://doi:10.1007/s00223-017-0372-2)  
689 [10.1007/s00223-017-0372-2](https://doi:10.1007/s00223-017-0372-2).

690

691 [3] Moore DD, Luu HH. Osteosarcoma. *Cancer Treat Res*. 162 (2014) 65-92. [https://doi:](https://doi:10.1007/978-3-319-07323-1_4)  
692 [10.1007/978-3-319-07323-1\\_4](https://doi:10.1007/978-3-319-07323-1_4).

693

694 [4] Kovac M, Blattmann C, Ribí S, Smida J, Mueller NS, Engert F, Castro-Giner F,  
695 Weischenfeldt J, Kovacova M, Krieg A, Andreou D, Tunn PU, Dürr HR, Rechl H, Schaser KD,  
696 Melcher I, Burdach S, Kulozik A, Specht K, Heinemann K, Fulda S, Bielack S, Jundt G,  
697 Tomlinson I, Korbel JO, Nathrath M, Baumhoer D. Exome sequencing of osteosarcoma reveals  
698 mutation signatures reminiscent of BRCA deficiency. *Nat Commun*. 6 (2015) 8940. [https://doi:](https://doi:10.1038/ncomms9940)  
699 [10.1038/ncomms9940](https://doi:10.1038/ncomms9940).

700

701 [5] Brown HK, Tellez-Gabriel M, Heymann D. Cancer stem cells in osteosarcoma. *Cancer Lett*.  
702 386 (2017) 189-195. [https://doi: 10.1016/j.canlet.2016.11.019](https://doi:10.1016/j.canlet.2016.11.019).

703

704 [6] Heymann MF, Lézet F, Heymann D. The contribution of immune infiltrates and the local  
705 microenvironment in the pathogenesis of osteosarcoma. *Cell Immunol*. 343 (2019) 103711.  
706 [https://doi: 10.1016/j.cellimm.2017.10.011](https://doi:10.1016/j.cellimm.2017.10.011).

707

708 [7] Yang C, Tian Y, Zhao F, Chen Z, Su P, Li Y, Qian A. Bone Microenvironment and  
709 Osteosarcoma Metastasis. *Int J Mol Sci*. 21 (2020) 6985. [https://doi: 10.3390/ijms21196985](https://doi:10.3390/ijms21196985).

710

711 [8] Cui J, Dean D, Hornicek FJ, Chen Z, Duan Z. The role of extracellular matrix in osteosarcoma  
712 progression and metastasis. *J Exp Clin Cancer Res*. 39 (2020) 178. [https://doi: 10.1186/s13046-](https://doi:10.1186/s13046-020-01685-w)  
713 [020-01685-w](https://doi:10.1186/s13046-020-01685-w).

714

715 [9] Balamuth NJ, Womer RB. Ewing's sarcoma. *Lancet Oncol*. 11 (2010) 184-92. [https://doi:](https://doi:10.1016/S1470-2045(09)70286-4)  
716 [10.1016/S1470-2045\(09\)70286-4](https://doi:10.1016/S1470-2045(09)70286-4).

717

718 [10] Renzi S, Anderson ND, Light N, Gupta A. Ewing-like sarcoma: An emerging family of  
719 round cell sarcomas. *J Cell Physiol*. 234 (2019) 7999-8007. [https://doi: 10.1002/jcp.27558](https://doi:10.1002/jcp.27558).

720  
721 [11] Tirode F, Laud-Duval K, Prieur A, Delorme B, Charbord P, Delattre O. Mesenchymal stem  
722 cell features of Ewing tumors. *Cancer Cell*. 11 (2007) 421-9. [https://doi:](https://doi:10.1016/j.ccr.2007.02.027)  
723 [10.1016/j.ccr.2007.02.027](https://doi:10.1016/j.ccr.2007.02.027).  
724  
725 [12] Todorova R. Ewing's sarcoma cancer stem cell targeted therapy. *Curr Stem Cell Res Ther*. 9  
726 (2014) 46-62. [https://doi: 10.2174/1574888x08666131203123125](https://doi:10.2174/1574888x08666131203123125).  
727  
728 [13] Lamhamedi-Cherradi SE, Santoro M, Ramammoorthy V, Menegaz BA, Bartholomeusz G,  
729 Iles LR, Amin HM, Livingston JA, Mikos AG, Ludwig JA. 3D tissue-engineered model of  
730 Ewing's sarcoma. *Adv Drug Deliv Rev*. 79-80 (2014) 155-71. [https://doi:](https://doi:10.1016/j.addr.2014.07.012)  
731 [10.1016/j.addr.2014.07.012](https://doi:10.1016/j.addr.2014.07.012).  
732  
733 [14] Yu H, Ge Y, Guo L, Huang L. Potential approaches to the treatment of Ewing's sarcoma.  
734 *Oncotarget*. 8 (2017) 5523-5539. [https://doi: 10.18632/oncotarget.12566](https://doi:10.18632/oncotarget.12566).  
735  
736 [15] Chow WA. Chondrosarcoma: biology, genetics, and epigenetics. *F1000Res*. 7 (2018) 1826.  
737 [https://doi: 10.12688/f1000research.15953.1](https://doi:10.12688/f1000research.15953.1).  
738  
739 [16] Mery B, Espenel S, Guy JB, Rancoule C, Vallard A, Aloy MT, Rodriguez-Lafrasse C,  
740 Magné N. Biological aspects of chondrosarcoma: Leaps and hurdles. *Crit Rev Oncol Hematol*.  
741 123 (2018) 32-36. [https://doi: 10.1016/j.critrevonc.2018.03.009](https://doi:10.1016/j.critrevonc.2018.03.009).  
742  
743 [17] Shupp AB, Kolb AD, Bussard KM. Novel Techniques to Study the Bone-Tumor  
744 Microenvironment. *Adv Exp Med Biol*. 1225 (2020) 1-18. [https://doi: 10.1007/978-3-030-35727-](https://doi:10.1007/978-3-030-35727-6_1)  
745 [6\\_1](https://doi:10.1007/978-3-030-35727-6_1).  
746  
747 [18] Roux, W. Beiträge zur Entwicklungsmechanik des Embryo. *Z. Biol*. 21 (1885) 411  
748  
749 [19] Harrison, R.G. The outgrowth of the nerve fiber as a mode of protoplasmic movement. *J Exp*  
750 *Zool*. 142 (1910) 5-73.  
751  
752 [20] Koledova Z. 3D Cell Culture: An Introduction. *Methods Mol Biol*. 1612 (2017) 1-11.  
753 [https://doi: 10.1007/978-1-4939-7021-6\\_1](https://doi:10.1007/978-1-4939-7021-6_1).  
754  
755 [21] Sitarski AM, Fairfield H, Falank C, Reagan MR. 3d Tissue Engineered In Vitro Models Of  
756 Cancer In Bone. *ACS Biomater Sci Eng*. 4 (2018) 324-336. [https://doi:](https://doi:10.1021/acsbomaterials.7b00097)  
757 [10.1021/acsbomaterials.7b00097](https://doi:10.1021/acsbomaterials.7b00097).  
758  
759 [22] Qiao, H., Tang, T. Engineering 3D approaches to model the dynamic microenvironments of  
760 cancer bone metastasis. *Bone Res*. 6 (2018) 3. <https://doi.org/10.1038/s41413-018-0008-9>.  
761  
762 [23] Chaicharoenaudomrung N, Kunhorm P, Noisa P. Three-dimensional cell culture systems as  
763 an *in vitro* platform for cancer and stem cell modeling. *World J Stem Cells*. 11 (2019) 1065-  
764 1083. [https://doi: 10.4252/wjsc.v11.i12.1065](https://doi:10.4252/wjsc.v11.i12.1065).

- 765 [24] De Luca A, Raimondi L, Salamanna F, Carina V, Costa V, Bellavia D, Alessandro R, Fini  
766 M, Giavaresi G. Relevance of 3d culture systems to study osteosarcoma environment. *J Exp Clin*  
767 *Cancer Res.* 37 (2018) 2. [https://doi: 10.1186/s13046-017-0663-5](https://doi.org/10.1186/s13046-017-0663-5).  
768
- 769 [25] Kelm, J.M., Timmins, N.E., Brown, C.J., Fussenegger, M. and Nielsen, L.K. Method for  
770 generation of homogeneous multicellular tumor spheroids applicable to a wide variety of cell  
771 types. *Biotechnol. Bioeng.* 83 (2003) 173-180. <https://doi.org/10.1002/bit.10655>.  
772
- 773 [26] Foty R. A simple hanging drop cell culture protocol for generation of 3D spheroids. *J Vis*  
774 *Exp.* 51 (2011) 2720. [https://doi: 10.3791/2720](https://doi.org/10.3791/2720).  
775
- 776 [27] Potter SW, Morris JE. Development of mouse embryos in hanging drop culture. *Anat Rec.*  
777 211 (1985) 48-56. [https://doi: 10.1002/ar.1092110109](https://doi.org/10.1002/ar.1092110109).  
778
- 779 [28] Reed BH, McMillan SC, Chaudhary R. The preparation of *Drosophila* embryos for live-  
780 imaging using the hanging drop protocol. *J Vis Exp.* 25 (2009) 1206. [https://doi: 10.3791/1206](https://doi.org/10.3791/1206).  
781
- 782 [29] Archacka K, Pozzobon M, Repele A, Rossi CA, Campanella M, De Coppi P. Culturing  
783 muscle fibres in hanging drop: a novel approach to solve an old problem. *Biol Cell.* 106 (2014)  
784 72-82. [https://doi: 10.1111/boc.201300028](https://doi.org/10.1111/boc.201300028).  
785
- 786 [30] Wang S, Wang X, Boone J, Wie J, Yip KP, Zhang J, Wang L, Liu R. Application of  
787 Hanging Drop Technique for Kidney Tissue Culture. *Kidney Blood Press Res.* 42 (2017) 220-  
788 231. [https://doi: 10.1159/000476018](https://doi.org/10.1159/000476018).  
789
- 790 [31] Panek M, Grabacka M, Pierzchalska M. The formation of intestinal organoids in a hanging  
791 drop culture. *Cytotechnology.* 70 (2018) 1085-1095. [https://doi: 10.1007/s10616-018-0194-8](https://doi.org/10.1007/s10616-018-0194-8).  
792
- 793 [32] Huang SW, Tzeng SC, Chen JK, Sun JS, Lin FH. A Dynamic Hanging-Drop System for  
794 Mesenchymal Stem Cell Culture. *Int J Mol Sci.* 21 (2020) 4298. [https://doi:](https://doi.org/10.3390/ijms21124298)  
795 [10.3390/ijms21124298](https://doi.org/10.3390/ijms21124298).  
796
- 797 [33] Carletti E, Motta A, Migliaresi C. Scaffolds for tissue engineering and 3D cell culture.  
798 *Methods Mol Biol.* 695 (2011) 17-39. [https://doi: 10.1007/978-1-60761-984-0\\_2](https://doi.org/10.1007/978-1-60761-984-0_2).  
799
- 800 [34] Kamatar A, Gunay G, Acar H. Natural and Synthetic Biomaterials for Engineering  
801 Multicellular Tumor Spheroids. *Polymers (Basel).* 12 (2020) 2506. [https://doi:](https://doi.org/10.3390/polym12112506)  
802 [10.3390/polym12112506](https://doi.org/10.3390/polym12112506).  
803
- 804 [35] Kureshi AK, Afoke A, Wohler S, Barker S, Brown RA. 3D culture model of fibroblast-  
805 mediated collagen creep to identify abnormal cell behaviour. *Biomech Model Mechanobiol.* 14  
806 (2015) 1255-63. [https://doi: 10.1007/s10237-015-0672-2](https://doi.org/10.1007/s10237-015-0672-2).  
807  
808
- 809 [36] Shahin-Shamsabadi A, Selvaganapathy PR. A rapid biofabrication technique for self-  
810 assembled collagen-based multicellular and heterogeneous 3D tissue constructs. *Acta Biomater.*  
811 92 (2019) 172-183. [https://doi: 10.1016/j.actbio.2019.05.024](https://doi.org/10.1016/j.actbio.2019.05.024).

812  
813  
814 [37] Kleinman HK, Martin GR. Matrigel: basement membrane matrix with biological activity.  
815 *Semin Cancer Biol.* 15 (2005) 378-86. [https://doi: 10.1016/j.semcancer.2005.05.004](https://doi.org/10.1016/j.semcancer.2005.05.004).  
816  
817 [38] Aoki S, Takezawa T, Sugihara H, Toda S. Progress in cell culture systems for pathological  
818 research. *Pathol Int.* 66 (2016) 554-562. [https://doi: 10.1111/pin.12443](https://doi.org/10.1111/pin.12443).  
819  
820 [39] Andersen T, Auk-Emblem P, Dornish M. 3D Cell Culture in Alginate Hydrogels.  
821 *Microarrays (Basel).* 4 (2015) 33-61. [https://doi: 10.3390/microarrays4020133](https://doi.org/10.3390/microarrays4020133).  
822  
823 [40] Fujita S, Wakuda Y, Matsumura M, Suye SI. Geometrically customizable alginate hydrogel  
824 nanofibers for cell culture platforms. *J Mater Chem B.* 7 (2019) 6556-6563. [https://doi: 10.1039/c9tb01353a](https://doi.org/10.1039/c9tb01353a).  
825  
826  
827 [41] Xu K, Ganapathy K, Andl T, Wang Z, Copland JA, Chakrabarti R, Florczyk SJ. 3D porous  
828 chitosan-alginate scaffold stiffness promotes differential responses in prostate cancer cell lines.  
829 *Biomaterials.* 217 (2019) 119311. [https://doi: 10.1016/j.biomaterials.2019.119311](https://doi.org/10.1016/j.biomaterials.2019.119311).  
830  
831 [42] Gao F, Li J, Wang L, Zhang D, Zhang J, Guan F, Yao M. Dual-enzymatically crosslinked  
832 hyaluronic acid hydrogel as a long-time 3D stem cell culture system. *Biomed Mater.* 15 (2020)  
833 045013. [https://doi: 10.1088/1748-605X/ab712e](https://doi.org/10.1088/1748-605X/ab712e).  
834  
835 [43] Maleki Dana P, Hallajzadeh J, Asemi Z, Mansournia MA, Yousefi B. Chitosan applications  
836 in studying and managing osteosarcoma. *Int J Biol Macromol.* 169 (2021) 321-329. doi:  
837 [10.1016/j.ijbiomac.2020.12.058](https://doi.org/10.1016/j.ijbiomac.2020.12.058).  
838  
839 [44] Aisenbrey EA, Murphy WL. Synthetic alternatives to Matrigel. *Nat Rev Mater.* 5 (2020)  
840 539-551. [https://doi: 10.1038/s41578-020-0199-8](https://doi.org/10.1038/s41578-020-0199-8).  
841  
842 [45] Park MH, Moon HJ, Park JH, Shinde UP, Ko du Y, Jeong B. PEG-Poly(L-alanine)  
843 thermogel as a 3D scaffold of bone-marrow-derived mesenchymal stem cells. *Macromol Biosci.*  
844 15 (2015) 464-72. [https://doi: 10.1002/mabi.201400426](https://doi.org/10.1002/mabi.201400426).  
845  
846 [46] Song H , Yang G , Huang P , Kong D , Wang W . Self-assembled PEG-poly(l-valine)  
847 hydrogels as promising 3D cell culture scaffolds. *J Mater Chem B.* 5 (2017) 1724-1733.  
848 [https://doi: 10.1039/c6tb02969h](https://doi.org/10.1039/c6tb02969h).  
849  
850 [47] Pradhan S, Hassani I, Seeto WJ, Lipke EA. PEG-fibrinogen hydrogels for three-dimensional  
851 breast cancer cell culture. *J Biomed Mater Res A.* 105 (2017) 236-252. [https://doi: 10.1002/jbm.a.35899](https://doi.org/10.1002/jbm.a.35899).  
852  
853  
854 [48] Wang Y, Cao X, Ma M, Lu W, Zhang B, Guo Y. A GelMA-PEGDA-nHA Composite  
855 Hydrogel for Bone Tissue Engineering. *Materials (Basel).* 13 (2020) 3735. [https://doi: 10.3390/ma13173735](https://doi.org/10.3390/ma13173735).  
856  
857

- 858 [49] Bhatia SN, Ingber DE. Microfluidic organs-on-chips. *Nat Biotechnol.* 32 (2014) 760-72.  
859 <https://doi: 10.1038/nbt.2989>.  
860
- 861 [50] Mehling M, Tay S. Microfluidic cell culture. *Curr Opin Biotechnol.* 25 (2014) 95-102.  
862 <https://doi: 10.1016/j.copbio.2013.10.005>.  
863
- 864 [51] Byambaa B, Annabi N, Yue K, Trujillo-de Santiago G, Alvarez MM, Jia W, Kazemzadeh-  
865 Narbat M, Shin SR, Tamayol A, Khademhosseini A. Bioprinted Osteogenic and Vasculogenic  
866 Patterns for Engineering 3D Bone Tissue. *Adv Healthc Mater.* 6 (2017) [https://doi:](https://doi: 10.1002/adhm.201700015)  
867 [10.1002/adhm.201700015](https://doi: 10.1002/adhm.201700015).  
868
- 869 [52] Mittal R, Woo FW, Castro CS, Cohen MA, Karanxha J, Mittal J, Chhibber T, Jhaveri VM.  
870 Organ-on-chip models: Implications in drug discovery and clinical applications. *J Cell Physiol.*  
871 234 (2019) 8352-8380. <https://doi: 10.1002/jcp.27729>.  
872
- 873 [53] Suarez-Martinez AD, Sole-Gras M, Dykes SS, Wakefield ZR, Bauer K, Majbour D, Bundy  
874 A, Pampo C, Burow ME, Siemann DW, Huang Y, Murfee WL. Bioprinting on Live Tissue for  
875 Investigating Cancer Cell Dynamics. *Tissue Eng Part A.* (2020). [https://doi:](https://doi: 10.1089/ten.TEA.2020.0190)  
876 [10.1089/ten.TEA.2020.0190](https://doi: 10.1089/ten.TEA.2020.0190). Online ahead of print.  
877
- 878 [54] Brennan MD, Rexus-Hall ML, Elgass LJ, Eddington DT. Oxygen control with  
879 microfluidics. *Lab Chip.* 14 (2014) 4305-18. <https://doi: 10.1039/c4lc00853g>.  
880
- 881 [55] Ahn J, Lim J, Jusoh N, Lee J, Park TE, Kim Y, Kim J, Jeon NL. 3D Microfluidic Bone  
882 Tumor Microenvironment Comprised of Hydroxyapatite/Fibrin Composite. *Front Bioeng*  
883 *Biotechnol.* 7 (2019) 168. <https://doi: 10.3389/fbioe.2019.00168>.  
884
- 885 [56] Desyatnik I, Krasner M, Frolov L, Ronen M, Guy O, Wasserman D, Tzur A, Avrahami D,  
886 Barbiro-Michaely E, Gerber D. An Integrated Microfluidics Approach for Personalized Cancer  
887 Drug Sensitivity and Resistance Assay. *Adv Biosyst.* 3 (2019) e1900001. [https://doi:](https://doi: 10.1002/adbi.201900001)  
888 [10.1002/adbi.201900001](https://doi: 10.1002/adbi.201900001).  
889
- 890 [57] Bersini S, Jeon JS, Dubini G, Arrigoni C, Chung S, Charest JL, Moretti M, Kamm RD. A  
891 microfluidic 3D in vitro model for specificity of breast cancer metastasis to bone. *Biomaterials.*  
892 35 (2014) 2454-61. <https://doi: 10.1016/j.biomaterials.2013.11.050>.  
893
- 894 [58] Almela T, Al-Sahaf S, Brook IM, Khoshroo K, Rasouljanboroujeni M, Fahimipour F,  
895 Tahriri M, Dashtimoghadam E, Bolt R, Tayebi L, Moharamzadeh K. 3D printed tissue  
896 engineered model for bone invasion of oral cancer. *Tissue Cell.* 52 (2018) 71-77. [https://doi:](https://doi: 10.1016/j.tice.2018.03.009)  
897 [10.1016/j.tice.2018.03.009](https://doi: 10.1016/j.tice.2018.03.009).  
898
- 899 [59] Wragg NM, Mosqueira D, Blokpeol-Ferreras L, Capel A, Player DJ, Martin NRW, Liu Y,  
900 Lewis MP. Development of a 3D Tissue-Engineered Skeletal Muscle and Bone Co-culture  
901 System. *Biotechnol J.* 15 (2020) e1900106. <https://doi: 10.1002/biot.201900106>.  
902
- 903 [60] Yang C, Tian Y, Zhao F, Chen Z, Su P, Li Y, Qian A. Bone Microenvironment and  
904 Osteosarcoma Metastasis. *Int J Mol Sci.* 21 (2020) 6985. <https://doi: 10.3390/ijms21196985>.

905  
906 [61] Rimann M, Laternser S, Gvozdenovic A, Muff R, Fuchs B, Kelm JM, Graf-Hausner U. An  
907 in vitro osteosarcoma 3D microtissue model for drug development. *J Biotechnol.* 189 (2014) 129-  
908 35. [https://doi: 10.1016/j.jbiotec.2014.09.005](https://doi.org/10.1016/j.jbiotec.2014.09.005).  
909  
910 [62] Baek N, Seo OW, Kim M, Hulme J, An SS. Monitoring the effects of doxorubicin on 3D-  
911 spheroid tumor cells in real-time. *Onco Targets Ther.* 9 (2016) 7207-7218. [https://doi:](https://doi.org/10.2147/OTT.S112566)  
912 [10.2147/OTT.S112566](https://doi.org/10.2147/OTT.S112566).  
913  
914 [63] León IE, Cadavid-Vargas JF, Resasco A, Maschi F, Ayala MA, Carbone C, Etcheverry SB.  
915 In vitro and in vivo antitumor effects of the VO-chrysin complex on a new three-dimensional  
916 osteosarcoma spheroids model and a xenograft tumor in mice. *J Biol Inorg Chem.* 21 (2016)  
917 1009-1020. [https://doi: 10.1007/s00775-016-1397-0](https://doi.org/10.1007/s00775-016-1397-0).  
918  
919 [64] Thanindratarn P, Li X, Dean DC, Nelson SD, Hornicek FJ, Duan Z. Establishment and  
920 Characterization of a Recurrent Osteosarcoma Cell Line: OSA 1777. *J Orthop Res.* 38 (2020)  
921 902-910. [https://doi: 10.1002/jor.24528](https://doi.org/10.1002/jor.24528).  
922  
923 [65] Lenna S, Bellotti C, Duchi S, Martella E, Columbaro M, Dozza B, Ballestri M, Guerrini A,  
924 Sotgiu G, Frisoni T, Cevolani L, Varchi G, Ferrari M, Donati DM, Lucarelli E. Mesenchymal  
925 stromal cells mediated delivery of photoactive nanoparticles inhibits osteosarcoma growth in  
926 vitro and in a murine in vivo ectopic model. *J Exp Clin Cancer Res.* 39 (2020) 40. [https://doi:](https://doi.org/10.1186/s13046-020-01548-4)  
927 [10.1186/s13046-020-01548-4](https://doi.org/10.1186/s13046-020-01548-4).  
928  
929 [66] Kiss A, Ráduly AP, Regdon Z, Polgár Z, Tarapcsák S, Sturniolo I, El-Hamoly T, Virág L,  
930 Hegedűs C. Targeting Nuclear NAD<sup>+</sup> Synthesis Inhibits DNA Repair, Impairs Metabolic  
931 Adaptation and Increases Chemosensitivity of U-2OS Osteosarcoma Cells. *Cancers (Basel).* 12  
932 (2020) 1180. [https://doi: 10.3390/cancers12051180](https://doi.org/10.3390/cancers12051180).  
933  
934 [67] Netti PA, Berk DA, Swartz MA, Grodzinsky AJ, Jain RK. Role of extracellular matrix  
935 assembly in interstitial transport in solid tumors. *Cancer Res.* 60 (2000) 2497-503.  
936  
937 [68] Akeda K, Nishimura A, Satonaka H, Shintani K, Kusuzaki K, Matsumine A, Kasai Y,  
938 Masuda K, Uchida A. Three-dimensional alginate spheroid culture system of murine  
939 osteosarcoma. *Oncol Rep.* 22 (2009) 997-1003. [https://doi: 10.3892/or\\_00000527](https://doi.org/10.3892/or_00000527).  
940  
941 [69] Tan PH, Chia SS, Toh SL, Goh JC, Nathan SS. Three-dimensional spatial configuration of  
942 tumour cells confers resistance to chemotherapy independent of drug delivery. *J Tissue Eng*  
943 *Regen Med.* 10 (2016) 637-46. [https://doi: 10.1002/term.1800](https://doi.org/10.1002/term.1800).  
944  
945 [70] Belisario DC, Akman M, Godel M, Campani V, Patrizio MP, Scotti L, Hattinger CM, De  
946 Rosa G, Donadelli M, Serra M, Kopecka J, Riganti C. ABCA1/ABCB1 Ratio Determines  
947 Chemo- and Immune-Sensitivity in Human Osteosarcoma. *Cells.* 9 (2020) 647. [https://doi:](https://doi.org/10.3390/cells9030647)  
948 [10.3390/cells9030647](https://doi.org/10.3390/cells9030647).  
949  
950 [71] Jiang T, Zhao J, Yu S, Mao Z, Gao C, Zhu Y, Mao C, Zheng L. Untangling the response of  
951 bone tumor cells and bone forming cells to matrix stiffness and adhesion ligand density by means

952 of hydrogels. *Biomaterials*. 188 (2019) 130-143. [https://doi: 10.1016/j.biomaterials.2018.10.015](https://doi.org/10.1016/j.biomaterials.2018.10.015).  
953 Erratum in: *Biomaterials*. 231(2020) 119663.  
954  
955 [72] Jiang T, Xu G, Chen X, Huang X, Zhao J, Zheng L. Impact of Hydrogel Elasticity and  
956 Adherence on Osteosarcoma Cells and Osteoblasts. *Adv Healthc Mater*. 8 (2019) e1801587.  
957 [https://doi: 10.1002/adhm.201801587](https://doi.org/10.1002/adhm.201801587). Erratum in: *Adv Healthc Mater*. (9) 2020 e2000054.  
958  
959 [73] Molina ER, Chim LK, Salazar MC, Mehta SM, Menegaz BA, Lamhamedi-Cherradi SE,  
960 Satish T, Mohiuddin S, McCall D, Zaska AM, Cuglievan B, Lazar AJ, Scott DW, Grande-Allen  
961 JK, Ludwig JA, Mikos AG. Mechanically tunable coaxial electrospun models of YAP/TAZ  
962 mechanoresponse and IGF-1R activation in osteosarcoma. *Acta Biomater*. 100 (2019) 38-51.  
963 [https://doi: 10.1016/j.actbio.2019.09.029](https://doi.org/10.1016/j.actbio.2019.09.029).  
964  
965 [74] Fallica B, Maffei JS, Villa S, Makin G, Zaman M. Alteration of cellular behavior and  
966 response to PI3K pathway inhibition by culture in 3D collagen gels. *PLoS One*. 7 (2012) e48024.  
967 [https://doi: 10.1371/journal.pone.0048024](https://doi.org/10.1371/journal.pone.0048024).  
968  
969 [75] Marastoni S, Ligresti G, Lorenzon E, Colombatti A, Mongiat M. Extracellular matrix: a  
970 matter of life and death. *Connect Tissue Res*. 49 (2008) 203-6. [https://doi:](https://doi.org/10.1080/03008200802143190)  
971 [10.1080/03008200802143190](https://doi.org/10.1080/03008200802143190).  
972  
973 [76] Charoen KM, Fallica B, Colson YL, Zaman MH, Grinstaff MW. Embedded multicellular  
974 spheroids as a biomimetic 3D cancer model for evaluating drug and drug-device combinations.  
975 *Biomaterials*. 35 (2014) 2264-71. [https://doi: 10.1016/j.biomaterials.2013.11.038](https://doi.org/10.1016/j.biomaterials.2013.11.038).  
976  
977 [77] Bai C, Yang M, Fan Z, Li S, Gao T, Fang Z. Associations of chemo- and radio-resistant  
978 phenotypes with the gap junction, adhesion and extracellular matrix in a three-dimensional  
979 culture model of soft sarcoma. *J Exp Clin Cancer Res*. 34 (2015) 58. doi: 10.1186/s13046-015-  
980 0175-0.  
981  
982 [78] Palubeckaitė I, Crooks L, Smith DP, Cole LM, Bram H, Le Maitre C, Clench MR, Cross  
983 NA. Mass spectrometry imaging of endogenous metabolites in response to doxorubicin in a novel  
984 3D osteosarcoma cell culture model. *J Mass Spectrom*. 55 (2020) e4461. [https://doi:](https://doi.org/10.1002/jms.4461)  
985 [10.1002/jms.4461](https://doi.org/10.1002/jms.4461).  
986  
987 [79] Green DW, Kim EJ, Jung HS. Spontaneous gene transfection of human bone cells using 3D  
988 mineralized alginate-chitosan macrocapsules. *J Biomed Mater Res A*. 103 (2015) 2855-63.  
989 [https://doi: 10.1002/jbm.a.35414](https://doi.org/10.1002/jbm.a.35414).  
990  
991 [80] Gorgun C, Ozturk S, Gokalp S, Vatansever S, Gurhan SI, Urkmez AS. Synergistic role of  
992 three dimensional niche and hypoxia on conservation of cancer stem cell phenotype. *Int J Biol*  
993 *Macromol*. 90 (2016) 20-6. [https://doi: 10.1016/j.ijbiomac.2015.12.053](https://doi.org/10.1016/j.ijbiomac.2015.12.053).  
994  
995 [81] Barbato L, Bocchetti M, Di Biase A, Regad T. Cancer Stem Cells and Targeting Strategies.  
996 *Cells*. 8 (2019) 926. [https://doi: 10.3390/cells8080926](https://doi.org/10.3390/cells8080926).  
997

998 [82] Vallette FM, Olivier C, Lézot F, Oliver L, Cochonneau D, Lalier L, Cartron PF, Heymann  
999 D. Dormant, quiescent, tolerant and persister cells: Four synonyms for the same target in cancer.  
1000 *Biochem Pharmacol.* 162 (2019) 169-176. [https://doi: 10.1016/j.bcp.2018.11.004](https://doi.org/10.1016/j.bcp.2018.11.004).  
1001  
1002 [83] Ozturk S, Gorgun C, Gokalp S, Vatansever S, Sendemir A. Development and  
1003 characterization of cancer stem cell-based tumoroids as an osteosarcoma model. *Biotechnol*  
1004 *Bioeng.* 117 (2020) 2527-2539. [https://doi: 10.1002/bit.27381](https://doi.org/10.1002/bit.27381).  
1005  
1006 [84] Bassi G, Panseri S, Dozio SM, Sandri M, Campodoni E, Dapporto M, Sprio S, Tampieri A,  
1007 Montesi M. Scaffold-based 3D cellular models mimicking the heterogeneity of osteosarcoma  
1008 stem cell niche. *Sci Rep.* 10 (2020) 22294. [https://doi: 10.1038/s41598-020-79448-y](https://doi.org/10.1038/s41598-020-79448-y).  
1009  
1010 [85] Tornín J, Villasante A, Solé-Martí X, Ginebra MP, Canal C. Osteosarcoma tissue-  
1011 engineered model challenges oxidative stress therapy revealing promoted cancer stem cell  
1012 properties. *Free Radic Biol Med.* 164 (2021) 107-118. [https://doi:](https://doi.org/10.1016/j.freeradbiomed.2020.12.437)  
1013 [10.1016/j.freeradbiomed.2020.12.437](https://doi.org/10.1016/j.freeradbiomed.2020.12.437).  
1014  
1015 [86] Gebhard C, Miller I, Hummel K, Neschi Née Ondrovics M, Schlosser S, Walter I.  
1016 Comparative proteome analysis of monolayer and spheroid culture of canine osteosarcoma cells.  
1017 *J Proteomics.* 177 (2018) 124-136. [https://doi: 10.1016/j.jprot.2018.01.006](https://doi.org/10.1016/j.jprot.2018.01.006).  
1018  
1019 [87] Trojani C, Weiss P, Michiels JF, Vinatier C, Guicheux J, Daculsi G, Gaudray P, Carle GF,  
1020 Rochet N. Three-dimensional culture and differentiation of human osteogenic cells in an  
1021 injectable hydroxypropylmethylcellulose hydrogel. *Biomaterials.* 26 (2005) 5509-17. [https://doi:](https://doi.org/10.1016/j.biomaterials.2005.02.001)  
1022 [10.1016/j.biomaterials.2005.02.001](https://doi.org/10.1016/j.biomaterials.2005.02.001).  
1023  
1024 [88] Turnbull G, Clarke J, Picard F, Riches P, Jia L, Han F, Li B, Shu W. 3D bioactive composite  
1025 scaffolds for bone tissue engineering. *Bioact Mater.* 3 (2017) 278-314. [https://doi:](https://doi.org/10.1016/j.bioactmat.2017.10.001)  
1026 [10.1016/j.bioactmat.2017.10.001](https://doi.org/10.1016/j.bioactmat.2017.10.001).  
1027  
1028 [89] Liu X, Jakus AE, Kural M, Qian H, Engler A, Ghaedi M, Shah R, Steinbacher DM,  
1029 Niklason LE. Vascularization of Natural and Synthetic Bone Scaffolds. *Cell Transplant.* 27  
1030 (2018) 1269-1280. [https://doi: 10.1177/0963689718782452](https://doi.org/10.1177/0963689718782452).  
1031  
1032 [90] Picone G, Cappadone C, Pasini A, Lovecchio J, Cortesi M, Farruggia G, Lombardo M,  
1033 Gianoncelli A, Mancini L, Ralf H M, Donato S, Giordano E, Malucelli E, Iotti S. Analysis of  
1034 Intracellular Magnesium and Mineral Depositions during Osteogenic Commitment of 3D  
1035 Cultured Saos2 Cells. *Int J Mol Sci.* 21 (2020) 2368. [https://doi: 10.3390/ijms21072368](https://doi.org/10.3390/ijms21072368).  
1036  
1037 [91] Prideaux M, Wijenayaka AR, Kumarasinghe DD, Ormsby RT, Evdokiou A, Findlay DM,  
1038 Atkins GJ. SaOS2 Osteosarcoma cells as an in vitro model for studying the transition of human  
1039 osteoblasts to osteocytes. *Calcif Tissue Int.* 95 (2014) 183-93. [https://doi: 10.1007/s00223-014-](https://doi.org/10.1007/s00223-014-9879-y)  
1040 [9879-y](https://doi.org/10.1007/s00223-014-9879-y).  
1041  
1042 [92] Kihara T, Umezu C, Sawada K, Furutani Y. Osteogenic cells form mineralized particles, a  
1043 few  $\mu\text{m}$  in size, in a 3D collagen gel culture. *PeerJ.* 7 (2019) e7889. [https://doi:](https://doi.org/10.7717/peerj.7889)  
1044 [10.7717/peerj.7889](https://doi.org/10.7717/peerj.7889).

1045  
1046 [93] Couchourel D, Escoffier C, Rohanizadeh R, Bohic S, Daculsi G, Fortun Y, Padrines M.  
1047 Effects of fibronectin on hydroxyapatite formation. *J Inorg Biochem.* 73 (1999) 129-36.  
1048 [https://doi: 10.1016/s0162-0134\(99\)00006-9](https://doi.org/10.1016/s0162-0134(99)00006-9).  
1049  
1050 [94] Padrines M, Rohanizadeh R, Damiens C, Heymann D, Fortun Y. Inhibition of apatite  
1051 formation by vitronectin. *Connect Tissue Res.* 41 (2000) 101-8. [https://doi:](https://doi.org/10.3109/03008200009067662)  
1052 [10.3109/03008200009067662](https://doi.org/10.3109/03008200009067662).  
1053  
1054 [95] Rohanizadeh R, Padrines M, Bouler JM, Couchourel D, Fortun Y, Daculsi G. Apatite  
1055 precipitation after incubation of biphasic calcium-phosphate ceramic in various solutions:  
1056 influence of seed species and proteins. *J Biomed Mater Res.* 42 (1998) 530-9. [https://doi:](https://doi.org/10.1002/(sici)1097-4636(19981215)42:4<530::aid-jbm8>3.0.co;2-6)  
1057 [10.1002/\(sici\)1097-4636\(19981215\)42:4<530::aid-jbm8>3.0.co;2-6](https://doi.org/10.1002/(sici)1097-4636(19981215)42:4<530::aid-jbm8>3.0.co;2-6).  
1058  
1059 [96] Vanderburgh JP, Guelcher SA, Sterling JA. 3D bone models to study the complex physical  
1060 and cellular interactions between tumor and the bone microenvironment. *J Cell Biochem.* 119  
1061 (2018) 5053-5059. [https://doi: 10.1002/jcb.26774](https://doi.org/10.1002/jcb.26774).  
1062  
1063 [97] Stoppato M, Carletti E, Maniglio D, Migliaresi C, Motta A. Functional role of scaffold  
1064 geometries as a template for physiological ECM formation: evaluation of collagen 3D assembly.  
1065 *J Tissue Eng Regen Med.* 7 (2013) 161-8. [https://doi: 10.1002/term.516](https://doi.org/10.1002/term.516).  
1066  
1067 [98] Riesco R, Boyer L, Blossé S, Lefebvre PM, Assemat P, Leichle T, Accardo A, Malaquin L.  
1068 Water-in-PDMS Emulsion Templating of Highly Interconnected Porous Architectures for 3D  
1069 Cell Culture. *ACS Appl Mater Interfaces.* 11 (2019) 28631-28640. [https://doi:](https://doi.org/10.1021/acsami.9b07564)  
1070 [10.1021/acsami.9b07564](https://doi.org/10.1021/acsami.9b07564).  
1071  
1072 [99] Sarkar S, Peng CC, Tung YC. Comparison of VEGF-A secretion from tumor cells under  
1073 cellular stresses in conventional monolayer culture and microfluidic three-dimensional spheroid  
1074 models. *PLoS One.* 15 (2020) e0240833. [https://doi: 10.1371/journal.pone.0240833](https://doi.org/10.1371/journal.pone.0240833).  
1075  
1076 [100] Gorska M, Krzywiec PB, Kuban-Jankowska A, Zmijewski M, Wozniak M, Wierzbička J,  
1077 Piotrowska A, Siwicka K. Growth Inhibition of Osteosarcoma Cell Lines in 3D Cultures: Role of  
1078 Nitrosative and Oxidative Stress. *Anticancer Res.* 36 (2016) 221-9.  
1079  
1080 [101] Gamblin AL, Renaud A, Charrier C, Hulin P, Louarn G, Heymann D, Trichet V, Layrolle  
1081 P. Osteoblastic and osteoclastic differentiation of human mesenchymal stem cells and monocytes  
1082 in a miniaturized three-dimensional culture with mineral granules. *Acta Biomater.* 10 (2014)  
1083 5139-5147. [https://doi: 10.1016/j.actbio.2014.08.033](https://doi.org/10.1016/j.actbio.2014.08.033).  
1084  
1085 [102] Sasmazel HT. Novel hybrid scaffolds for the cultivation of osteoblast cells. *Int J Biol*  
1086 *Macromol.* 49 (2011) 838-46. [https://doi: 10.1016/j.ijbiomac.2011.07.022](https://doi.org/10.1016/j.ijbiomac.2011.07.022).  
1087  
1088 [103] Zafeiris K, Brasinika D, Karatza A, Koumoulos E, Karoussis IK, Kyriakidou K, Charitidis  
1089 CA. Additive manufacturing of hydroxyapatite-chitosan-genipin composite scaffolds for bone  
1090 tissue engineering applications. *Mater Sci Eng C Mater Biol Appl.* 119 (2021) 111639.  
1091 [https://doi: 10.1016/j.msec.2020.111639](https://doi.org/10.1016/j.msec.2020.111639).

1092  
1093 [104] Chen C, Chen K, Yang ST. Effects of three-dimensional culturing on osteosarcoma cells  
1094 grown in a fibrous matrix: analyses of cell morphology, cell cycle, and apoptosis. *Biotechnol*  
1095 *Prog.* 19 (2003) 1574-82. [https://doi: 10.1021/bp034024w](https://doi.org/10.1021/bp034024w).  
1096  
1097 [105] Thai VL, Griffin KH, Thorpe SW, Randall RL, Leach JK. Tissue engineered platforms for  
1098 studying primary and metastatic neoplasm behavior in bone. *J Biomech.* 115 (2021) 110189.  
1099 [https://doi: 10.1016/j.jbiomech.2020.110189](https://doi.org/10.1016/j.jbiomech.2020.110189).  
1100  
1101 [106] Hao S, Ha L, Cheng G, Wan Y, Xia Y, Sosnoski DM, Mastro AM, Zheng SY. A  
1102 Spontaneous 3D Bone-On-a-Chip for Bone Metastasis Study of Breast Cancer Cells. *Small.* 14  
1103 (2018) e1702787. [https://doi: 10.1002/sml.201702787](https://doi.org/10.1002/sml.201702787).  
1104  
1105 [107] Choudhary S, Ramasundaram P, Dziopa E, Mannion C, Kissin Y, Tricoli L, Albanese C,  
1106 Lee W, Zilberberg J. Human ex vivo 3D bone model recapitulates osteocyte response to  
1107 metastatic prostate cancer. *Sci Rep.* 8 (2018) 17975. [https://doi: 10.1038/s41598-018-36424-x](https://doi.org/10.1038/s41598-018-36424-x).  
1108  
1109 [108] Raman PS, Paul CD, Stroka KM, Konstantopoulos K. Probing cell traction forces in  
1110 confined microenvironments. *Lab Chip.* 13 (2013) 4599-607. [https://doi: 10.1039/c3lc50802a](https://doi.org/10.1039/c3lc50802a).  
1111  
1112 [109] Chaddad H, Kuchler-Bopp S, Fuhrmann G, Gegout H, Ubeaud-Sequier G, Schwinté P,  
1113 Bornert F, Benkirane-Jessel N, Idoux-Gillet Y. Combining 2D angiogenesis and 3D  
1114 osteosarcoma microtissues to improve vascularization. *Exp Cell Res.* 360 (2017) 138-145.  
1115 [https://doi: 10.1016/j.yexcr.2017.08.035](https://doi.org/10.1016/j.yexcr.2017.08.035).  
1116  
1117 [110] Massimini M, De Maria R, Malatesta D, Romanucci M, D'Anselmo A, Della Salda L.  
1118 Establishment of three-dimensional canine osteosarcoma cell lines showing vasculogenic  
1119 mimicry and evaluation of biological properties after treatment with 17-AAG. *Vet Comp Oncol.*  
1120 17 (2019) 376-384. [https://doi: 10.1111/vco.12482](https://doi.org/10.1111/vco.12482).  
1121  
1122 [111] Fong EL, Lamhamedi-Cherradi SE, Burdett E, Ramamoorthy V, Lazar AJ, Kasper FK,  
1123 Farach-Carson MC, Vishwamitra D, Demicco EG, Menegaz BA, Amin HM, Mikos AG, Ludwig  
1124 JA. Modeling Ewing sarcoma tumors in vitro with 3D scaffolds. *Proc Natl Acad Sci U S A.* 110  
1125 (2013) 6500-5. [https://doi: 10.1073/pnas.1221403110](https://doi.org/10.1073/pnas.1221403110).  
1126  
1127 [112] Boehme KA, Nitsch J, Riester R, Handgretinger R, Schleicher SB, Kluba T, Traub F.  
1128 Arsenic trioxide potentiates the effectiveness of etoposide in Ewing sarcomas. *Int J Oncol.* 49  
1129 (2016) 2135-2146. [https://doi: 10.3892/ijo.2016.3700](https://doi.org/10.3892/ijo.2016.3700).  
1130  
1131 [113] Santoro M, Lamhamedi-Cherradi SE, Menegaz BA, Ludwig JA, Mikos AG. Flow  
1132 perfusion effects on three-dimensional culture and drug sensitivity of Ewing sarcoma. *Proc Natl*  
1133 *Acad Sci U S A.* 112 (2015) 10304-9. [https://doi: 10.1073/pnas.1506684112](https://doi.org/10.1073/pnas.1506684112).  
1134  
1135 [114] Molina ER, Chim LK, Salazar MC, Koons GL, Menegaz BA, Ruiz-Velasco A,  
1136 Lamhamedi-Cherradi SE, Vetter AM, Satish T, Cuglievan B, Smoak MM, Scott DW, Ludwig  
1137 JA, Mikos AG. 3D Tissue-Engineered Tumor Model for Ewing's Sarcoma That Incorporates

1138 Bone-like ECM and Mineralization. *ACS Biomater Sci Eng.* 6 (2020) 539-552. [https://doi:](https://doi:10.1021/acsbiomaterials.9b01068)  
1139 10.1021/acsbiomaterials.9b01068.  
1140  
1141 [115] Marturano-Kruik A, Villasante A, Yaeger K, Ambati SR, Chramiec A, Raimondi MT,  
1142 Vunjak-Novakovic G. Biomechanical regulation of drug sensitivity in an engineered model of  
1143 human tumor. *Biomaterials.* 150 (2018) 150-161. [https://doi: 10.1016/j.biomaterials.2017.10.020](https://doi:10.1016/j.biomaterials.2017.10.020).  
1144  
1145 [116] May WA, Grigoryan RS, Keshelava N, Cabral DJ, Christensen LL, Jenabi J, Ji L, Triche  
1146 TJ, Lawlor ER, Reynolds CP. Characterization and drug resistance patterns of Ewing's sarcoma  
1147 family tumor cell lines. *PLoS One.* 8 (2013) e80060. [https://doi: 10.1371/journal.pone.0080060](https://doi:10.1371/journal.pone.0080060).  
1148  
1149 [117] Leuchte K, Altvater B, Hoffschlag S, Potratz J, Meltzer J, Clemens D, Luecke A, Harges J,  
1150 Dirksen U, Juergens H, Kailayangiri S, Rossig C. Anchorage-independent growth of Ewing  
1151 sarcoma cells under serum-free conditions is not associated with stem-cell like phenotype and  
1152 function. *Oncol Rep.* 32 (2014) 845-52. [https://doi: 10.3892/or.2014.3269](https://doi:10.3892/or.2014.3269).  
1153  
1154 [118] Villasante A, Marturano-Kruik A, Vunjak-Novakovic G. Bioengineered human tumor  
1155 within a bone niche. *Biomaterials.* 35 (2014) 5785-94. [https://doi:](https://doi:10.1016/j.biomaterials.2014.03.081)  
1156 10.1016/j.biomaterials.2014.03.081.  
1157  
1158 [119] Marturano-Kruik A, Villasante A, Vunjak-Novakovic G. Bioengineered Models of Solid  
1159 Human Tumors for Cancer Research. *Methods Mol Biol.* 1502 (2016) 203-11. [https://doi:](https://doi:10.1007/7651_2016_353)  
1160 10.1007/7651\_2016\_353. Erratum in: *Methods Mol Biol.* 1502 (2016) E1  
1161  
1162 [120] Riffle S, Pandey RN, Albert M, Hegde RS. Linking hypoxia, DNA damage and  
1163 proliferation in multicellular tumor spheroids. *BMC Cancer.* 17 (2017) 338. [https://doi:](https://doi:10.1186/s12885-017-3319-0)  
1164 10.1186/s12885-017-3319-0.  
1165  
1166 [121] Domenici G, Eduardo R, Castillo-Ecija H, Orive G, Montero Carcaboso Á, Brito C. PDX-  
1167 Derived Ewing's Sarcoma Cells Retain High Viability and Disease Phenotype in Alginate  
1168 Encapsulated Spheroid Cultures. *Cancers (Basel).* 13 (2021) 879. [https://doi:](https://doi:10.3390/cancers13040879)  
1169 10.3390/cancers13040879.  
1170  
1171 [122] Riffle S, Hegde RS. Modeling tumor cell adaptations to hypoxia in multicellular tumor  
1172 spheroids. *J Exp Clin Cancer Res.* 36 (2017) 102. [https://doi: 10.1186/s13046-017-0570-9](https://doi:10.1186/s13046-017-0570-9).  
1173  
1174 [123] David E, Blanchard F, Heymann MF, De Pinieux G, Gouin F, Rédini F, Heymann D. The  
1175 Bone Niche of Chondrosarcoma: A Sanctuary for Drug Resistance, Tumour Growth and also a  
1176 Source of New Therapeutic Targets. *Sarcoma.* 2011 (2011) 932451. [https://doi:](https://doi:10.1155/2011/932451)  
1177 10.1155/2011/932451.  
1178  
1179 [124] Evans HL, Ayala AG, Romsdahl MM. Prognostic factors in chondrosarcoma of bone: a  
1180 clinicopathologic analysis with emphasis on histologic grading. *Cancer.* 40 (1977) 818-31.  
1181 [https://doi: 10.1002/1097-0142\(197708\)40:2<818::aid-cnrcr2820400234>3.0.co;2-b](https://doi:10.1002/1097-0142(197708)40:2<818::aid-cnrcr2820400234>3.0.co;2-b).  
1182  
1183 [125] Boeuf S, Steck E, Peltari K, Hennig T, Buneb A, Benz K, Witte D, Sülmann H, Poustka  
1184 A, Richter W. Subtractive gene expression profiling of articular cartilage and mesenchymal stem

1185 cells: serpins as cartilage-relevant differentiation markers. *Osteoarthritis Cartilage*. 16 (2008) 48-  
1186 60. [https://doi: 10.1016/j.joca.2007.05.008](https://doi.org/10.1016/j.joca.2007.05.008).  
1187  
1188 [126] Boeuf S, Kunz P, Hennig T, Lehner B, Hogendoorn P, Bovée J, Richter W. A  
1189 chondrogenic gene expression signature in mesenchymal stem cells is a classifier of conventional  
1190 central chondrosarcoma. *J Pathol*. 216 (2008) 158-66. [https://doi: 10.1002/path.2389](https://doi.org/10.1002/path.2389).  
1191  
1192 [127] Monderer D, Luseau A, Bellec A, David E, Ponsolle S, Saiagh S, Bercegeay S, Piloquet P,  
1193 Denis MG, Lodé L, Rédini F, Biger M, Heymann D, Heymann MF, Le Bot R, Gouin F,  
1194 Blanchard F. New chondrosarcoma cell lines and mouse models to study the link between  
1195 chondrogenesis and chemoresistance. *Lab Invest*. 93 (2013) 1100-14. [https://doi:](https://doi.org/10.1038/labinvest.2013.101)  
1196 [10.1038/labinvest.2013.101](https://doi.org/10.1038/labinvest.2013.101).  
1197  
1198 [128] van Oosterwijk JG, Herpers B, Meijer D, Briaire-de Bruijn IH, Cleton-Jansen AM,  
1199 Gelderblom H, van de Water B, Bovée JV. Restoration of chemosensitivity for doxorubicin and  
1200 cisplatin in chondrosarcoma in vitro: BCL-2 family members cause chemoresistance. *Ann Oncol*.  
1201 23 (2012) 1617-26. [https://doi: 10.1093/annonc/mdr512](https://doi.org/10.1093/annonc/mdr512).  
1202  
1203 [129] Reijnders CM, Waaijer CJ, Hamilton A, Buddingh EP, Dijkstra SP, Ham J, Bakker E,  
1204 Szuhai K, Karperien M, Hogendoorn PC, Stringer SE, Bovée JV. No haploinsufficiency but loss  
1205 of heterozygosity for EXT in multiple osteochondromas. *Am J Pathol*. 177 (2010) 1946-57.  
1206 [https://doi: 10.2353/ajpath.2010.100296](https://doi.org/10.2353/ajpath.2010.100296).  
1207  
1208 [130] Voissiere A, Jouberton E, Maubert E, Degoul F, Peyrode C, Chezal JM, Miot-Noirault É.  
1209 Development and characterization of a human three-dimensional chondrosarcoma culture for in  
1210 vitro drug testing. *PLoS One*. 12 (2017) e0181340. [https://doi: 10.1371/journal.pone.0181340](https://doi.org/10.1371/journal.pone.0181340).  
1211  
1212 [131] Voissiere A, Weber V, Gerard Y, Rédini F, Raes F, Chezal JM, Degoul F, Peyrode C,  
1213 Miot-Noirault E. Proteoglycan-targeting applied to hypoxia-activated prodrug therapy in  
1214 chondrosarcoma: first proof-of-concept. *Oncotarget*. 8 (2017) 95824-95840. [https://doi:](https://doi.org/10.18632/oncotarget.21337)  
1215 [10.18632/oncotarget.21337](https://doi.org/10.18632/oncotarget.21337).  
1216  
1217 [132] Peyrode C, Weber V, David E, Vidal A, Auzeloux P, Communal Y, Dauplat MM, Besse S,  
1218 Gouin F, Heymann D, Chezal JM, Rédini F, Miot-Noirault E. Quaternary ammonium-melphalan  
1219 conjugate for anticancer therapy of chondrosarcoma: in vitro and in vivo preclinical studies.  
1220 *Invest New Drugs*. 30 (2012) 1782-90. [https://doi: 10.1007/s10637-011-9663-z](https://doi.org/10.1007/s10637-011-9663-z).  
1221  
1222 [133] Perut F, Sbrana FV, Avnet S, De Milito A, Baldini N. Spheroid-based 3D cell cultures  
1223 identify salinomycin as a promising drug for the treatment of chondrosarcoma. *J Orthop Res*.  
1224 2018. [https://doi: 10.1002/jor.23880](https://doi.org/10.1002/jor.23880). Online ahead of print.  
1225  
1226 [134] Lhuissier E, Bazille C, Aury-Landas J, Girard N, Pontin J, Boittin M, Boumediene K,  
1227 Baugé C. Identification of an easy to use 3D culture model to investigate invasion and anticancer  
1228 drug response in chondrosarcomas. *BMC Cancer*. 17 (2017) 490. [https://doi: 10.1186/s12885-](https://doi.org/10.1186/s12885-017-3478-z)  
1229 [017-3478-z](https://doi.org/10.1186/s12885-017-3478-z).  
1230

1231 [135] Palubeckaitė I, Venneker S, Briaire-de Bruijn IH, van den Akker BE, Krol AD, Gelderblom  
1232 H, Bovée JVMG. Selection of Effective Therapies Using Three-Dimensional *in vitro* Modeling  
1233 of Chondrosarcoma. *Front Mol Biosci.* 7 (2020) 566291. [https://doi:](https://doi:10.3389/fmolb.2020.566291)  
1234 10.3389/fmolb.2020.566291.  
1235  
1236 [136] Hamdi DH, Barbieri S, Chevalier F, Groetz JE, Legendre F, Demoor M, Galera P, Lefaix  
1237 JL, Saintigny Y. In vitro engineering of human 3D chondrosarcoma: a preclinical model relevant  
1238 for investigations of radiation quality impact. *BMC Cancer.* 15 (2015) 579. [https://doi:](https://doi:10.1186/s12885-015-1590-5)  
1239 10.1186/s12885-015-1590-5.  
1240  
1241 [137] Vautier D, Hemmerlé J, Vodouhe C, Koenig G, Richert L, Picart C, Voegel JC, Debry C,  
1242 Chluba J, Ogier J. 3-D surface charges modulate protrusive and contractile contacts of  
1243 chondrosarcoma cells. *Cell Motil Cytoskeleton.* 56 (2003) 147-58. [https://doi:](https://doi:10.1002/cm.10140)  
1244 10.1002/cm.10140.  
1245  
1246 [138] Minopoli M, Sarno S, Di Carluccio G, Azzaro R, Costantini S, Fazioli F, Gallo M, Apice  
1247 G, Cannella L, Rea D, Stoppelli MP, Boraschi D, Budillon A, Scotlandi K, De Chiara A, Carriero  
1248 MV. Inhibiting Monocyte Recruitment to Prevent the Pro-Tumoral Activity of Tumor-Associated  
1249 Macrophages in Chondrosarcoma. *Cells.* 9 (2020) 1062. [https://doi: 10.3390/cells9041062.](https://doi:10.3390/cells9041062)  
1250  
1251 [139] Carriero MV, Bifulco K, Minopoli M, Lista L, Maglio O, Mele L, Di Carluccio G, De Rosa  
1252 M, Pavone V. UPARANT: a urokinase receptor-derived peptide inhibitor of VEGF-driven  
1253 angiogenesis with enhanced stability and in vitro and in vivo potency. *Mol Cancer Ther.* 13  
1254 (2014) 1092-104. [https://doi: 10.1158/1535-7163.MCT-13-0949.](https://doi:10.1158/1535-7163.MCT-13-0949)  
1255  
1256 [140] Parfenov VA, Mironov VA, van Kampen KA, Karalkin PA, Koudan EV, Pereira FD,  
1257 Petrov SV, Nezhurina EK, Petrov OF, Myasnikov MI, Walboomers FX, Engelkamp H,  
1258 Christianen P, Khesuani YD, Moroni L, Mota C. Scaffold-free and label-free biofabrication  
1259 technology using levitational assembly in a high magnetic field. *Biofabrication.* 12 (2020)  
1260 045022. [https://doi: 10.1088/1758-5090/ab7554.](https://doi:10.1088/1758-5090/ab7554)  
1261  
1262  
1263  
1264  
1265  
1266  
1267  
1268  
1269

**Table 1. 3D methods used in primary bone tumors**

Bone tumor	Technique	Material	Cell line	Reference
<b>Osteosarcoma</b>	Scaffold-free	Hanging drop and Low-attachment	SaOS2 HOS U2OS D17 MG63	61-66,83,84,86,109
	Scaffold	Alginate beads	LM8 MG63	68,72,78,83
		Silk sponge	SaOS2 HOS	69
		PEG	SaOS2	71
		Collagen	MG63 U2OS	72,74,76,90-94,110
		Agarose	MG63	72
		PCL	MG63	73,102
		Methylcellulose	HOS	77
		PLA	MG63	97
		HA BCP	MG63 OS MSC	84,85,102,107 101,107
Complex matrix	SaOS2 U2OS MG63	70,72,84,92		
Microfluidic/Bioprinting	PDMS	SaOS2 MG63	96,110 98,99,106-109	
<b>Ewing Sarcoma</b>	Scaffold-free	Hanging drop and Low attachment	RD-ES A673 SK-N-MC VH-64 T-32 TC-71 A4573	112,117-119
	Scaffold	PCL	TC-71	111,113,114
		Collagen	RD-ES A673 SK-N-MC	115
		HA	RD-ES A763 SK-N-MC	115
		Agar Alginate	A673 Primary cell lines	120 121,122
<b>Chondrosarcoma</b>	Scaffold-free	Hanging drop and Low attachment	SW1353 CAL78 OUMS27 CH03 CH34 CH56 CH2879	127-131,133

			L835	
		Levitation forces	SW1353	140
	Scaffold	Alginate	CH28979 JJ012 SW1353	134,135
		Collagen	SW1353	136,138
		Titanium beads	HCS-2/8	137

PEG: polyethylene glycol; PCL: poly( $\epsilon$ -caprolactone; PLA: poly(D,L-lactic acid; HA: Hydroxyapatite; BCP: biphasic calcium phosphate; PDMS: Polydimethylsiloxane

1270 **Figure Legends**

1271

1272 **Figure 1. Osteosarcoma spheroid.** Representative images of OS spheroid. A) HES staining of  
1273 MNNG/HOS spheroid. B) Wide-field MNNG/HOS spheroid using a Nikon Eclipse Ni  
1274 microscope. C) MNNG/HOS spheroid at day 3 obtained from 20,000 cells in DMEM (Gibco®)  
1275 supplemented with 1% L-glutamine plus 10% FVS using 96-well low adherent plate U-bottom  
1276 (ThermoFisher), labelled with Vybran™ DiO (ThermoFisher) and imaged in a Operetta CLS  
1277 microscope (PerkinElmer).

1278 **Figure 2. Sarcospheres from different OS cell lines.** Representative images of OS spheroid  
1279 formed from different OS cell lines depicting differences in size and morphology. MNNG-HOS  
1280 and MG63 OS cells were plated at 5,000 cells/well and 2,500 cell/well respectively in low  
1281 adhesion plates (Corning Costar®) coated with DMEM (Gibco®) + 10% agarose and imaged on  
1282 days 1-4 using the Celigo Imaging Cytometry System.

1283

1284 **Figure 3. 3D Spheroid PDMS chip.** PDMS microsystem for spheroid cell culture in a 60 x 22  
1285 mm slide. Microsystem is constituted by a reservoir for media (a 15 ml Falcon tube cut at desired  
1286 size) glued to the PDMS microsystem. The reservoir is connected to the cell culture chamber by  
1287 an 8 mm length channel (200 µm wide and 70 µm high). Cell culture chamber is 4 mm wide by  
1288 20 mm long (height 200 µm). To slowdown media flow, a 2 cm long serpentine channel (200 µm  
1289 wide 70 µm high) was placed after the cell chamber. Output through 1.5 mm Tygon tubing with  
1290 500 µm internal diameter.

1291

1292 **Figure 4. Cell subpopulation in an OS spheroid.** Spheroids are characterised by a continuum  
1293 subset of cells that goes from apoptotic or bone-like MSC non-dividing cells (in red) to a  
1294 peripheral proliferative subset of cells (green cells). 10,000 GFP-MNNG/HOS cells were seeded  
1295 into a 96-multiwells low-attachment plate and cultured for 13 days. Pictures showed population  
1296 evolution from day 5 to day 13. GFP expressing MNNG/HOS osteosarcoma cells stained with  
1297 DiD (ThermoFisher) to show the retention of DiD by a non-proliferating subpopulation of the

1298 cells in the formed spheroid and imaged using fluorescent microscopy. Scale bar corresponds to  
1299 50  $\mu\text{m}$ .

1300

1301

1302

1303

1304

**Figure 1**

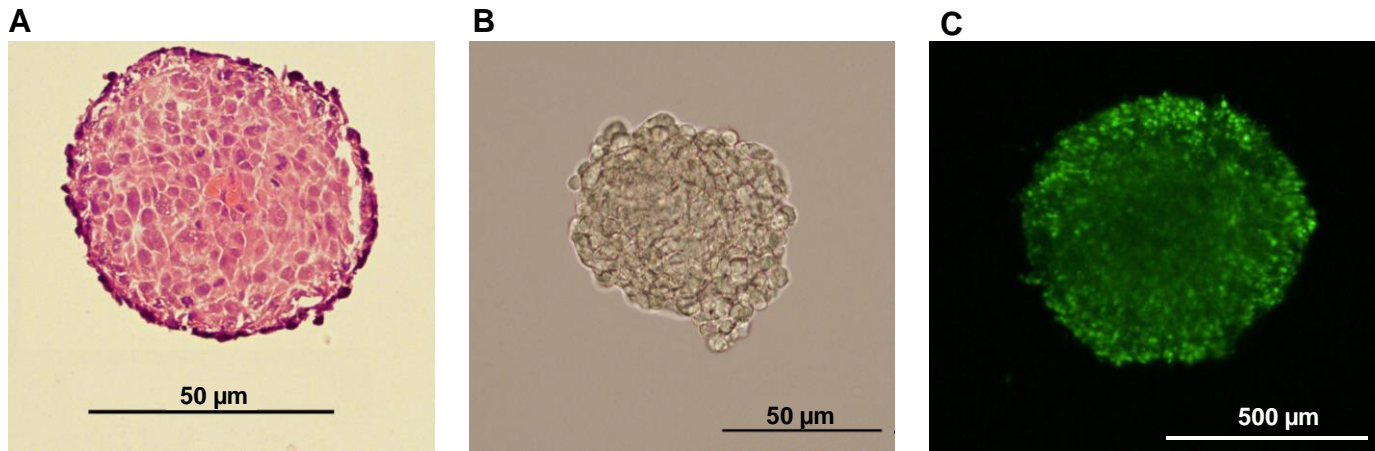


**Figure 2**

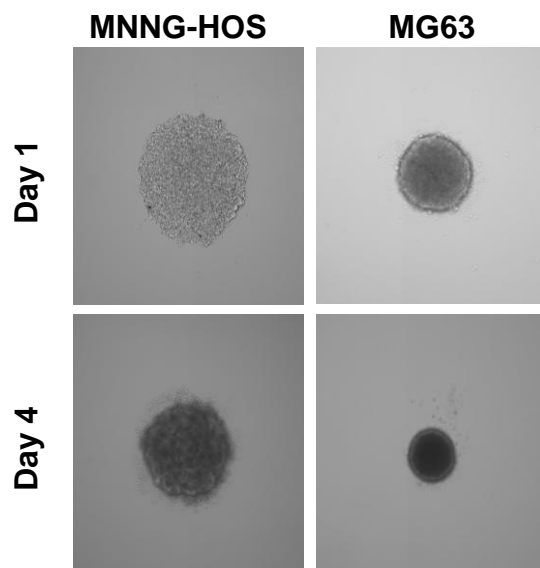


**Figure 3**

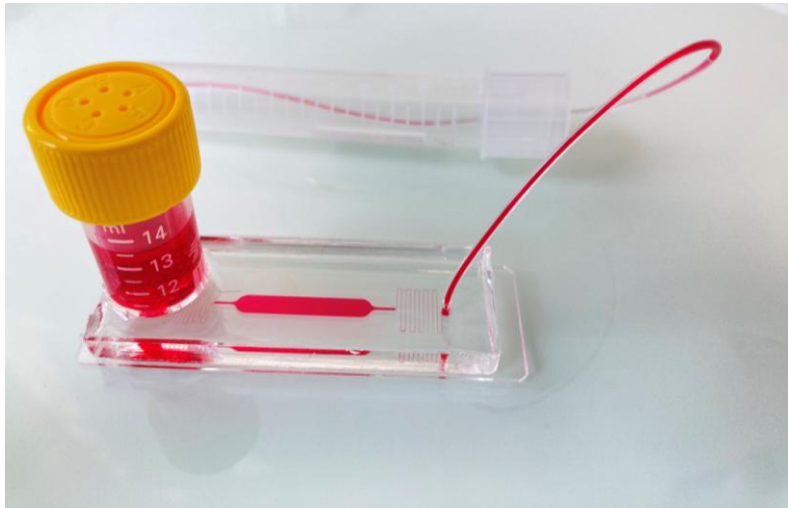
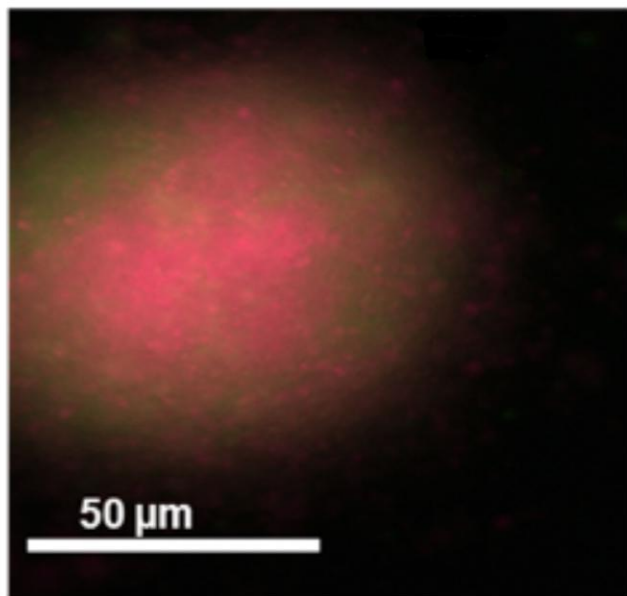


Figure 4

Day 5



Day 13

